ALEPH 94-069
MINIV 94-003
P. Coyle et al.
11.05.1994

Test Beam Results from Prototypes of the Upgraded ALEPH Vertex Detector

G. Bagliesi[7], G. Barber[5], G. Batignani[7], A.M. Bencheikh[6], F. Bosi[7], A. Bonissent[6], L. Bosisio[9], C. Bozzi[7], G. Bujosa[6], D. Calvet[6], W. Cameron[5], J. Carr[6], M. Carpinelli[7], M. Cattaneo[5], C. Colledani[11], P. Coyle[6], D. Creanza[1], M. De Palma[1], W. Dulinski[11], C. Diaconu[6], S. D'Auria[4], R. Dell'Orso[7], P. Dornan[5], P. Elmer[10], E. Focardi[3], F. Forti[7], M. Giorgi[7], D. Johnson[8], N. Konstantinidis[5], G. Maggi[1], M. Maggi[2], J. Nash[5], S. Nitzsche[2], W. Orejudos[10], V. O'Shea[4], G. Parrini[3], P. Payre[6], D. Price[5], C. Raine[4], G. Raso[1], G. Rizzo[7], L. Silvestris[1], K. Smith[4], P. Spagnolo[7], A. Stacey[5], P. Tempesta[1], G. Tonelli[7], R. Turchetta[11], P.G. Verdini[7], J. Walsh[7]

1) Dipartimento di Fisica, INFN Sezione di Bari, 70126 Bari, Italy 2) CERN, Geneva, Switzerland 3) University and INFN, Florence, Italy 4) University of Glasgow, U.K. 5) Imperial College, London, U.K. 6) Centre de Physique de Particules, Marseille, France 7) University, INFN and Scuola Normale Superiore, Pisa, Italy 8) Royal Holloway, U.K. 9) University and INFN, Trieste, Italy 10) University of Wisconsin, Madison, WI USA 11) LEPSI, Strasbourg, France

Abstract

Testbeam results obtained using prototypes of the upgraded ALEPH vertex detector are presented. In particular signal to noise measurements with MX7 and VIKING readout chips are given along with corresponding spatial resolutions. Performances obtained using two alternative readout schemes for the z side kapton fanout, daisy chain or variable pitch, are compared.

1 Introduction

In order to increase the efficiency for observing the Higgs via b quark tagging the ALEPH collaboration is in the process of upgrading its existing vertex detector. It is planned that the upgraded detector will be installed in the spring of 1995 in time for LEP II physics. The main improvements will be increased radiation hardness, increased solid angle coverage, improved spatial resolution and a reduced and more uniform material distribution.

The radiation hardness improvements will come from replacing the current CAMEX amplifier/multiplexer chip, radiation hard to about 10 krad, with a chip of radiation hardness better than 100 krad. Two chips have been considered; the MX7 chip developed at RAL [1] and the VIKING chip developed at CERN [2].

The amount of material presented by the detector will be reduced by relocating the z side readout electronics to the end of the detector rather than, as in the current Vdet, having them distributed in the sensitive region. To do this a fanout will be used to connect the z side strips to the z side electronics. In practice, due to the larger number of z strips (1920) than readout channels (1024), a reduction in the number of readout strips is required. Two alternative connection schemes on the fanout have been proposed to achieve this.

1. **Daisy Chain:** By connecting together strips at position Z and at Z+L/2, where L is the total length of the detector, the number of readout strips is reduced by a factor 2, but at the cost of introducing a two-fold ambiguity and increasing the noise due to the higher capacitance and lower bias resistance.

2. **Variable Pitch:** In principle the readout pitch of the silicon needs only to be less than or equal to the projected length of the track segment inside the silicon. As this varies as $t \times tan\theta$, where t is the thickness of the detector and θ is the angle of incidence of the track, one can change the readout pitch along the length of the detector to match the incidence angle of the track at its intersection with the detector. Using a constant pitch detector this can be achieved by connecting together adjacent detector strips onto the same strip of the fanout.

In order to measure the signal/noise performance, one of the important parameters that determined the final choice of readout chip, and to investigate the alternative connection schemes for the fanout, two prototype detector modules were constructed and evaluated in a testbeam. In the following note we describe the construction of the prototypes, the set up of the test beam used to collect the data, the analysis procedures and the performance of the prototypes as characterized by their measured signal/noise ratio and position resolutions. Finally a brief discussion on the final choice of readout chip and fanout design for the Vdet upgrade is given.

2 Hardware

2.1 The Prototypes

Figure 1 shows the layout of the prototype modules studied in the testbeam. The sensitive area consisted of three current ALEPH silicon strip detectors. These double-sided detectors, make use of the biasing scheme introduced in [5], and have been

designed by the Pisa group [6]. They were processed by CSEM, Neuchatel according to a fabrication process developed in common by INFN Pisa and CSEM. The active area of the 300 μm thick detector was 4.96 cm$\times$4.96 cm, with a total chip size of 5.12 cm$\times$5.12 cm. The strip pitch was 25 μm on the $r\phi$ side (p-side) and 50 μm on the z side (n-side). Although the readout pitch was 50 μm on the $r\phi$ side and 100 μm on the z side, the position resolution was improved by exploiting the capacitative charge division between intermediate 'floating' strips and the nearest readout strips. On the $r\phi$ side the three wafers were simply bonded together to form effective strips of three times the length. On the z side, the fanout was used to route the signals to the readout electronics at the end of the module.

The z side fanout, fabricated by Max Levi Autograph, Philadelphia, consisted of 50 μm thick kapton plated with 2.5 μm Cu/ 2 μm Ni strips. In addition the bonding pads were coated at CERN with 1 μm of Au. In order to test the two alternative bonding schemes discussed previously, the fanout was a "hybrid" design using daisy chain on two of the wafers and variable pitch on the third as shown in figure 2. In the variable pitch region the readout strip pitch increased by 100 μm every cm and within each region a number of different bonding patterns 1-of-1, 1-of-2 etc. were implemented as illustrated in figure 3.

The readout strips were coupled to the readout chips via the AC coupling chips designed for the L3 vertex detector. They also had a readout pitch of 50 μm and for these test modules did not include protection diodes against capacitor breakdown.

Two prototypes were built for the testbeam studies. One prototype used the MX7 chip and the other the VIKING chip. A total of twelve readout chips were used for each prototype, six on the $r\phi$ side and six on the z side, leading to a total of 768 readout channels per side.

The whole assembly was supported on a G10 frame and mounted on a rotatable platform in the testbeam.

2.2 Test Beam Setup

Both the MX7 and VIKING prototypes were irradiated by 100 GeV pions at the ALEPH X7 testbeam at CERN during a two week period in the summer of 1993.

To define the trajectory of each beam track, the Strasbourg beam telescope was used [3],[4]. As shown in figure 4, it consisted of eight reference planes orientated such that four planes measured the x coordinate and four planes measured the y coordinate. The prototypes were located between the references planes and usually both prototypes were readout simultaneously except at large incidence angles, where space constraints necessitated the removal of one or other of the prototypes.

The references planes were single-sided, AC-coupled, $3*6$ cm^2 silicon detectors with a readout pitch of 50 μm equiped with MX3 chips. Their analog signals, as well as those of the prototypes, were digitized using VME siroccos.

The data acquisition was controlled by a VME Eurocom 6 processor running OS9 and allowed online monitoring of interesting quantities such as signal/noise, beam profiles, etc. For each trigger, the raw data for all strips of the telescope planes and the prototypes were written onto an EXABYTE tape. A single event required about 18 kbytes.

The trigger was defined by the coincidence of the capture cycle of the MX3 chips

and scintillators at the entrance and exit of the telescope. Typically 30 triggers were taken every SPS spill and a typical run consisted of 20k triggers. Approximately 15 Gbytes of data were written to tape at incidence angles up to 53 degrees and at various positions on the prototypes.

3 Signal/Noise Analysis and Results

3.1 Cluster Finding

To form a cluster, the signal and noise of each strip was calculated on an event-by-event basis, taking into account possible common mode variation. Adjacent strips having a signal/noise greater than a certain threshold were then defined as a cluster and kept for further analysis. The details of the clustering procedure are now described.

3.1.1 Pedestals, common mode, signals, Noise

The raw data ADC count for the ith strip in the kth event was considered as a superposition of three contributions :

$$ADC^k(i) = S^k(i) + PED^k(i) + CMS^k(i)$$

where $S(i)$ represents the signal from the track ionization, $PED(i)$ is the ADC pedestal and CMS, the "common mode signal", is the joint noisy variation of the signal for all the strips on a given readout chip. Before beginning the computation of these components, strips previously identified as bad (noisy, disconnected or shorted) were excluded from the analysis.

The procedure used to compute the pedestal for each event and strip consisted of two steps :

1. **The initialisation** was done on the first 50 events for each run and the pedestals were computed as :

$$PED^{50}(i) = \frac{1}{50}\sum_{k=1}^{50} ADC^k(i)$$

2. **The updating** of the pedestals after the first 50 events was an iterative procedure which extracts the slowly varying component of the RAW data:

$$PED^k(i) = (1 - \frac{1}{50})PED^{k-1}(i) + \frac{1}{50}ADC^k(i) \qquad (k > 50)$$

Once the pedestal for each strip was known, the signal uncorrected for the common mode variations was calculated

$$S^{uncor}(i) = ADC^k(i) - PED^k(i).$$

The common mode for each event was then defined as the mean of this quantity averaged over 32 strips situated on the same physical chip, taking care to remove strips which may have had signal :

$$CMS^k_{32strips} = \frac{1}{32}\sum_{j=1}^{32} S^{uncor}(j)$$

Finally the signal on strip i for event k was given by:

$$S^k(i) = ADC^k(i) - PED^k(i) - CMS^k(i)$$

The noise was defined as the statistical fluctuation of this signal. The noise calculation was performed in two steps:

1. The next group of 50 events were used to **initialise** the noise:

$$N^{100}(i) = \sqrt{\frac{1}{50}\sum_{j=50}^{100}(S^j(i) - \bar{S}(i))^2}$$

   where $\bar{S}(i)$ is the mean of the signal for the strip i on the 50 events considered.

2. The **updating** of the noise was done using the same iterative procedure as is used in the pedestal calculation.

$$[N^k(i)]^2 = (1 - \frac{1}{50})[N^{k-1}(i)]^2 + \frac{1}{50}[S^k(i)]^2 \qquad (k > 100)$$

3.1.2 Forming the Cluster

Once the signal and noise for each strip of the detector was known, clusters of adjacent strips having a signal characteristic of a minimium ionizing particle were defined.

Before attempting to form a cluster it was necessary to make the correspondance between the sirocco channel and the geometrical position of the strips, thereby taking into account errors in the wire bonding and unbonded strips.

In order to speed up the search procedure, cluster seeds were first identified by means of a digital rectangular filter [3]. The initial length of the digital rectangular filter was modified during the seed search in order to identify possible charge deposition, via capacitance coupling, onto strips adjacent to a disconnected strip.

Having identified the seeds, a more detailed analysis was performed to isolate acceptable clusters:

1. Consider groups of strips centered on a seed and search for the strip j with the best signal-to-noise ratio. If the condition

$$\frac{S(j)}{N(j)} > (S/N)_{cut}^{central}$$

   is not satisfied, the procedure interrupts and re-starts with the next seed.

2. Starting from the seed strip, we move out (to the left and the right) strip by strip until the 'neighbour' cut is no longer satisfied:

$$\frac{S(j)}{N(j)} > (S/N)_{cut}^{neighbours}$$

   during this process bad strips are ignored, except if there are more than three bad strips in the cluster in which case the cluster is discarded.

Cuts	rϕ side		z side	
	MX7	VIKING	MX7	VIKING
Central strip S/N	5.	6.	3.	3.
Neighb. strip S/N	2.0	2.0	2.0	2.0
Cluster S/N	6.	10.	4.	4.
Max.nr. strips/clust.	10	10	10	10
Max.nr. of dead strips	3	3	3	3

Table 1: Cuts Used in the Cluster Search.

3. If the neighbour condition fails the cluster limits are fixed on the last accepted strips on the left and on the right. The number of strips accepted in the cluster, the cluster extent ($E^{cluster}$), cannot be greater than 10.

4. The cluster signal and noise were defined as:

$$S^{cluster} = \sum_{cluster} S(j)\delta_{j,good}$$

$$N^{cluster} = \sqrt{\frac{1}{E^{cluster}} \sum_{cluster} [N(j)]^2 \delta_{j,good}}$$

where $\delta_{j,good}$ means that the sum is taken only on the good strips. Finally, the accepted cluster had to satisfy :

$$\frac{S^{cluster}}{N^{cluster}} > (S/N)^{cluster}_{cut}$$

Table 1 summarises the values of the cuts used in the cluster search procedure.

3.2 Results for Signal, Noise, Signal/Noise

As previously mentioned, each prototype consisted of two regions; (1) the daisy chain region in which two detectors were multiplexed together and (2) the variable pitch region in which strips were ganged together in a configuration appropriate for the incidence angle of the track. In the following section we first discuss the signal, noise and signal/noise observed in the daisy chain region (rϕ side and z side) for both the MX7 and VIKING readout chips. Then using the variable pitch region of the VIKING prototype the effects of the various bonding schemes are studied. The results can be interpreted within the framework of the following qualitative arguments:

- **Noise:** The noise observed on a single strip is composed of a parallel and a series component. The parallel component is determined by the bias resistor and leakage current. It increases when several strips are connected. A factor of $\sqrt{2}$ is expected in the case of daisy chaining two strips. The series component is determined by the characteristics of the amplifier and the input capacitance. The latter increases linearly when several strips are connected together and is further increased if the fanout is present. An offset due to the intrinsic noise of the amplifier also needs to be added.

- **Signal:** The amount of signal observed increases with the incident track angle and, due to the loss of the signal to ground via the strip to ground capacitance, the signal collection will decrease as the number of floating strips between the readout strips increases. In addition, on the z side the fanout may introduce extra capacitance to ground leading to further loss of signal.

3.2.1 S/N: $r\phi$ Side, z Side (Daisy Chain)

Figure 5 shows the distribution of signal, noise and signal/noise obtained for both the MX7 and VIKING prototypes on the $r\phi$ side for tracks incident perpendicular to the detectors (0 degrees). The noise is reasonably Gaussian but has a small tail at large values. For the measurements reported here, clusters with a noise more than three sigma from the mean were discarded.

Due to different gains in the readout chain the means of the signal and noise distributions are different for the MX7 and VIKING. Taking the ratio of the signal/noise the gain differences cancel and the signal/noise performances of the two chips on the $r\phi$ side are seen to be similar. Figure 6 show the signal/noise distributions fitted to a Landau convoluted with a Gaussian. To quote the signal/noise we use the mean of these distribution: giving values of about 33 for the VIKING and 31 for the MX7 respectively.

Figure 7 shows the variation of the means of the signal, noise and signal/noise distributions measured on the $r\phi$ side as a function of the incident track angle. As expected, the noise is constant and the signal demonstrates a $1/cos\theta$ dependence. Also shown in figure 7 are the same quantities measured in the z side (daisy chain) region. The signal/noise is almost a factor of two lower than that observed on the $r\phi$ side. This is presumably due to the larger capacitance of the z side strips and the extra capacitance from the kapton fanout.

Figure 8 shows the clear pulse height correlation observed between the signals on the $r\phi$ and z sides.

3.2.2 S/N: z Side (Variable Pitch)

Figure 9 shows the noise dependence on angle and connection scheme for the variable pitch region on the z side of the VIKING detector. The noise is seen to increase as more strips are ganged together.

Figure 10 shows the corresponding dependence of the signal on angle and connection scheme. Also plotted as the solid curve is the maximum possible detectable signal calculated using the expected $1/cos\theta$ dependence normalized to the 1-of-1 point. The signal is observed to decrease as the number of floating strips increases.

Figure 11 shows the corresponding signal/noise dependence. It interesting to note that in the 1-of-1 region, in which a single strip is connected via the fanout, the signal/noise of about 27 is better than that observed in the z side daisy chain and approaches the value observed on the ϕ side. Also the trade off in signal and noise on connection scheme can be seen, for example although the signal is larger in the 2-of-2 case compared to the 1-of-2 case, the noise is also larger leading to a slightly lower signal/noise.

4 Position Resolution Analysis and Results

In order that the spatial resolution of the test detectors could be determined using the tracking information provided by the telescope, the entire test setup had first to be aligned to a very high precision. In practice this alignment was performed in two stages; first the eight planes of the telescope were aligned with respect to one another to provide a frame of reference for the test detectors and then the test detectors were aligned with respect to this frame of reference. This alignment procedure is described in detail below.

4.1 Aligning the Telescope

The telescope had four planes measuring x coordinates and four planes measuring y coordinates. In the following text these will be referred to as x or y plane number 1 to 4, where the numbering goes by increasing z. To transform these measured coordinates into a common frame of reference, it was necessary to align the telescope planes with respect to one another. In principle the relative misalignment of the planes included any combination of translational offsets along the x, y and z axes, rotational offsets in the xy, yz and xz planes. In practice several of these offsets could be ignored depending on the telescope planes under consideration. For example, translations along the z axis were considered negligible with respect to the distance between the planes, translations along the $x(y)$ axis were invisible to those planes measuring y (x) and the only important rotational offsets were those in the xy plane.

The alignment was performed in two steps: a single operation (the prealignment) corrected any gross translational offsets in the xy plane and then an iterative procedure removed the remaining translational and rotational offsets. For the prealignment the residual distributions for planes 2 and 3 were made using all the good hits in every good event in the run. The average offset of each residual distribution from zero was then applied as a correction to all of the good hits so that the residual distributions were centred on, or near zero. A good event was defined as having one hit per plane in the telescope and as producing tracks with a slope of less than 10^{-3}. After the prealignment the following iterative alignment procedure was applied.

1. Use the measured hits along with the current corrections (δ_x and δ_y) to make the residual distributions.

2. Make a Gaussian fit to the residual distributions to provide σ_{res}.

3. Loop over all the good hits and reject those which have a contribution to the residual distribution $> \sigma_{res} * N_{res}$. The factor N_{res} has an initial value of 5.0 and is reduced by 0.5 on each iteration down to a minimum of 3.0.

4. Use the remaining good hits to fill the distributions of x_{hit} against y_{pred} and y_{hit} against x_{pred} for planes 2 and 3. Line fits to these distributions are sensitive to translational offsets, via the intercept, and rotational offsets, via the slope.

5. Use the fit results to calculate new corrections according to

$$\delta_x = I_x + S_x * y_{pred}$$

and

$$\delta_y = I_y + S_y * x_{pred}$$

where I_x and S_x are the intercept and slope of the distribution using x_{hit} and I_y and S_y are the intercept and slope of the distribution using y_{hit}.

4.2 Aligning the Test Detectors

The aligned telescope provied two tracks per event; one using hits from the four planes measuring the x coordinate and the other using hits from the four planes measuring the y coordinate. When combined with measurements of the z positions of the test detectors and their angle(β) with respect to the nominal beam axis, these tracks can be used to predict hit positions in the test detectors in much the same way as was used in the alignment of the telescope planes. It was however found necessary to optimise both the measured z positions of the detectors as well as the angle β on a run by run basis in order to extract the best possible alignment. This involved stepping β and z through a reasonable range about their nominal values until a Gaussian fit to the residual distribution produced the minimum σ_{res} with a good χ^2.

The distribution of the difference between the predicted hit position and the actual hit position measured in the test detectors provides a measure of the detectors intrinsic resolution according to the relation:

$$\sigma_i = \sqrt{\sigma_{res}^2 - \sigma_{tk}^2 - \sigma_{mcs}^2}$$

Where σ_i is the intrinsic detector resolution, σ_{res} is the width of the measured residual distribution, σ_{tk} is the calculated uncertainty on the track extrapolations and σ_{mcs} is the calculated uncertainty due to multiple coulomb scattering in the material of the test setup.

4.3 Position Resolution Results

4.3.1 Position Algorithms

To calculate the position of the track impact from the cluster, two methods were used:

- **Centre of gravity:** The simple centre of gravity definition for the cluster position (X_{cl}) given by:

$$X_{cl} = \frac{\sum_{i=1}^{E} S_i X_i}{\sum_{i=1}^{E} S_i}$$

  where E is the cluster extent and S_i the signal on strip i having position X_i.

- η **Correction:** For the accepted clusters we define the so-called η function

$$\eta = \frac{S^{left}}{S^{left} + S^{right}}$$

  where S^{left} and S^{right} are the signals observed on the central strip and the neighbouring strip with the highest signal, taking into account the geometrical order of the strips. Figure 12 shows the typical distribution of η for perpendicular

tracks in a prototype detector. The density of hits ($dN/D\eta$) as a function of η has peaks near 0 and 1 corresponding to the readout strips and at 0.5 corresponding to the intermediate floating strip. The fact that the density of hits is non-uniform indicates that the charge division between the readout strips is non-linear with respect to the impact position of the track between the two strips. To correct for this non-linearity, and to therefore improve the resolution, the distribution of the integral of the normalised η distribution is formed (figure 13) and the quantity

$$f(\eta_0) = P \int_0^{\eta_0} \frac{dN}{d\eta}(\eta)_n d\eta$$

used as a lookup table to correct the position estimate calculated from the η integration. Here P is the readout pitch and $\frac{dN}{d\eta}(\eta)_n$ the normalised $\frac{dN}{d\eta}(\eta)$ distribution.

The final position is thus given by

$$X_{cl} = X_{left} + f(\eta)$$

For the telescope the position resolution of a single plane, using the η algorithm, was typically about 7 μm and led to an error on the line fit extrapolation (σ_{tk}) of about 3 μm. The error due to multiple coulomb scattering (σ_{mcs}) varied with the angle of the prototype detectors but was typically about 1 μm.

The projection of the shape of the charge distribution on the detector strips can also be derived from the $dN/d\eta$ distribution using the following formula [7]:

$$c(x) = \frac{1}{PdN/d\eta(x)_n}$$

where $c(x)$ is a normalised function describing the shape of the projected charge distribution. Figure 14 shows the spatial distrbution of the charge measured in this way for the VIKING detector and normal incidence tracks. The FWHM of the distribution is 9 μm on the $r\phi$ side and 11 μm on the z side.

4.3.2 Resolution: $r\phi$ Side, z Side (Daisy Chain)

Example residual distributions using the η method for the MX7 and VIKING prototypes on both the $r\phi$ and z sides (daisy chain) for perpendicular tracks are shown in Figure 15.

The final resolutions are calculated by fitting the residual distribution with a Gaussian plus a flat background and then subtracting in quadrature the track extrapolation error and the multiple coulomb scattering error from the sigma of the Gaussian. The constant term allows the small fraction of events in the tails to be taken into account in the fit.

Figure 16 shows the resolution for various slices of signal/noise. The resolution initially improve as the signal/noise increases, but then deteriorates rapidily for very large ionization deposits, indicating that the tails are due to delta ray production [8].

Figure 17 shows the position resolutions obtained as a function of track angle for the $r\phi$ side and z side (daisy chain) of the VIKING prototype. The resolutions obtained

using both the centre-of-gravity and η algorithms are shown. On the $r\phi$ side, the resolution is essentially constant with angle and is slightly better using the η algorithm (about 4 μm).

On the z side (daisy chain) the resolution deteriorates rapidily with angle. For angles less than 30 degrees the η algorithm performs best, while above 30 degrees the centre of gravity is best. The η algorithm is poor at large angles because in this regime, the cluster multiplicity is typically 5 or 6 strips and thus the central two strips of the cluster have the same pulse height apart from variations due to the noise.

4.3.3 Resolution: z Side (Variable Pitch)

Figure 18 shows the resolutions obtained for a variety of variable pitch bonding schemes as a function of angle. In all these cases, as the cluster multiplicity is small, the η algorithm is used. The best resolution is obtained using the 2-of-n bonding scheme at the large angles giving values of 8 μm at zero degrees increasing to 31 μm at 53 degrees.

Figure 19 shows the resolution measured using the 2-of-2 connection scheme at various angles and illustrates the importance of matching the track angle to the readout pitch in order to have the best resolution.

Figure 20 compares the resolution obtained in the daisy chain region to that obtained using the variable pitch bonding scheme giving the best resolution (2-of-n, when n¿1). Also shown is the z resolution measured in data with the current Vdet. For angles below 30 degrees the variable pitch resolution is about 20% better than the daisy chain. Above 30 degrees the resolutions are essentially the same.

5 Monte Carlo Simulation

A dedicated code was developed to simulate the configuration of the test beam. The appropriate routines were extracted from Galeph [9], and included into a simplified skeleton, along with the analysis routines for test beam data processing. The generation of the raw data comprises the following steps :

- compute the energy lost in the silicon by the incident pion. This depends upon the track energy and length of the track segment. At this level, the positions of the entry and exit points are also computed.
- generate the electron-hole pairs along the track, drift them towards the end faces of the wafer, together with lateral diffusion, and distribute them on the appropriate strips.
- compute the charge collected on the readout strips, either directly or by capacitive coupling.
- generate the noise on the readout strips. This is made of two components: the parallel noise originates from the detector components, and the series noise is generated inside the amplifier and fed back onto the readout strip via the feedback capacitor. The latter also generates some noise charge on the neighbouring strips, by capacitive coupling [10].

With respect to the standard Galeph routines, the following changes were made:

1. Landau fluctuations inside the silicon wafer were explicitly simulated. This was done by dividing the track element into 40 small segments. The energy deposited by each segment was calculated independently using the Geant routine GLANDZ, with a mean value of $3.86 MeV/cm$, (or a most probable value of $84 keV$ for $300 \mu m$ of silicon) [11]. No explicit delta-ray simulation was done.

2. The capacitive couplings for a readout pitch of $50 \mu m$ in $r\phi$ and $100 \mu m$ in z, and the VIKING amplifier, were recomputed using a code provided by P. Cattaneo, which solves the set of linear equations describing the capacitive network.

3. The daisy chain readout in the z direction was simulated by doubling the strip length in the computation of the strip capacitance. The coupling coefficients were kept unchanged. No attempt was to include the capacitive effects of the kapton.

4. for the $r\phi$ readout, the total strip length was multiplied by 3 for the same reason.

The data analysis was identical to that of real data. The clustering algorithms and thresholds were the same. The cluster position was computed by the centre of gravity method.

With the simulation described above, the signal to noise ratio appears to be significantly better than what is measured on the prototype, especially on the z face. For perpendicularly incident tracks, we obtain $S/N \simeq 30$ in z, $S/N \simeq 35$ in $r\phi$, to be compared with $S/N \simeq 18$ in z and $S/N \simeq 33$ in $r\phi$. These differences are believed to reflect some weakness either in the description of the processes by which the noise is generated, or in the values of the various capacitances which compose the network. Work is currently in progress to improve our knowledge of these problems. For the moment, we choose to increase the parallel noise in order to have the same total noise level at zero degrees as that observed in the data. When this is done, the agreement between the signal/noise ratios at other angles is very good.

Figure 21 shows the predicted resolution as a function of incidence angle, for both the $r\phi$ and z (daisy chain) sides after the noise has been tuned. The agreement between simulation and data is quite good.

Figure 22 shows a comparision in the z side of the same simulation program with and without taking into account the effect of the Landau fluctuations inside the wafer. As one can expect, this has no effect at zero degrees, where the cluster is made of one or two strips. At steeper angles, where the clusters become larger, the non-uniformity of the energy distribution has an effect similar to that of the electronic noise. In fact, the two effects are of the same order of magnitude at large angles. For example, at 45^o, $\sigma_{Landau} = \sigma_{Noise} = 17 \mu m$. It should be noted that the current simulation of the Aleph Vdet does not include this effect, and the same discrepancy is observed when comparing the position resolutions of Vdet for real data and Galeph events.

6 Discussion and Choices

6.1 Choice of Readout Chip

The final decision on which readout chip to use for the upgrade project was determined by a number of factors; radiation hardness, signal/noise, cost, availability etc. As the signal/noise performances of the MX7 and VIKING chips measured in the testbeam were found to be similar it was decided that radiation hardness should be the most important criterium. This was considered wise as the dose rates from beam injection or during beam tuning cannot be reliably predicted at LEP II and it is these rates which have caused the bulk of the damage experienced by the current Vdet.

The VIKING chip has been shown to have gentle performance degradation under irradiation, the main effect being a smooth increase in noise (less than a factor 2 at 200 krad). The performance of the standard MX7 chip, as used in the test beam, was measured to deteriorate significantly after a few tens of krads. Recently a radiation hard version of the MX7, using the Harris process, has become available and measurements show that this chip is insensitive to radiation up to the maximum tested dose of 200 krad. It is this latter chip which was therefore chosen for the upgrade. Although this chip was not explicitly evaluated in the test beam, subsequent bench measurements showed the signal/noise performances of the standard and radiation hard versions of the MX7 to be similar.

6.2 Choice of Connection Scheme for the Fanout

Although the variable pitch readout scheme yielded a 20% improvement in resolution as compared to the daisy chain scheme at low angles, its use for the upgraded ALEPH detector is less clear for the following reasons:

- In order to match the number of readout channels to the number of strips needed to be readout, the implementation of the variable pitch scheme for the upgraded ALEPH detector would required an increase in the intrinsic strip pitch, with a corresponding degradation in the resolution. This would also necessitate a redesign of the masks used in fabrication of the silicon wafers.

- Due to the finite size of the beam spot the track angle at a particular z distance along the silicon is not well defined.

This, combined with the increased complexity of the wire bonding pattern and the deterioration of two track resolution associated with variable pitch, made the small resolution improvement over the daisy chain scheme less attractive.

One disadvantage of the daisy chain method is the introduction of a second ghost hit 10 cm from the true hit. In practice, Monte Carlo studies show that the effect of this on b tagging is negligible [12]. Another disadvantage is the lower signal/noise ratio. To take full profit of the potentially higher signal/noise of the variable pitch scheme however, would require the design of several different detector layouts, with strips of different width. This would result in significantly higher cost and increased complexity of assembly. The daisy chain scheme was chosen for final use in the upgraded Vdet.

7 Conclusion

The signal to noise and resolution performances of two prototypes designed to test readout chips (MX7 or VIKING) and to help choose the connection scheme (daisy chain or variable pitch) for the z side fanout of the ALEPH microvertex detector upgrade have been reported.

On the $r\phi$ side, signal/noise of about 31 and 33 were measured for perpendicularly incident tracks using the MX7 and VIKING readout chips respectively. The corresponding position resolution were about 5 μm and 6 μm and found to be essentially independent of incident track angle.

On the z side, daisy chain region, the signal/noise for perpendicular tracks was almost a factor of two lower than that of the $r\phi$ side for both chips. The resolution on the z side deteriorated with increasing incident track angle; using the daisy chain connection scheme values of 11 μm at zero degrees increasing to about 33 μm at an angle of 53 degrees were observed. The resolutions obtained using the variable pitch connection scheme were 20% better for angles below 30 degrees.

The radiation hard MX7 chip and the daisy chain connection scheme for the z side fanout were chosen for use in the upgraded detector.

8 Acknowledgement

We gratefully thank W. Dulinski, C. Colledani and R. Turchetta for allowing us to use the marvelous Strasbourg beam telescope and data acquisition system. We thank A. Rudge for help in setting up the hardware and finally Jan Straver for his help with the offline software.

References

[1] P.P Allport, P. Seller and M. Tyndel, "A Low Power VLSI Multiplexed Amplifier for Silion Strip Detectors", Nucl. Instr. and Meth. A273, (1988) 630.

[2] P. Holl et al., "VIKING, a CMOS low noise monolithic 128 channel frontend for Si-strip detector readout", Nucl. Instr. and Meth. A340, (1994) 572.

[3] R. Turchetta, "Developpement de Detecteurs Silicium Double Face a Resolution Spatiale Elevee at Lecture Projective", These CRN/HE 91-07.

[4] J. Straver et al., "One Micron Spatial Resolution with Silicon Strip Detectors", CERN-PPE/94-26.

[5] P. Holl et al., "A Double Sided Silicon Strip Detector With Capacitative Readout and a New method of Integrated Bias Coupling", IEEE Trans. Nucl. Sci. NS-36, 251 (1989).

[6] G. Batignani et al., "Development and Performance od Double Sided Silicon Strip Detectors", Nucl. Instr. and Meth. A310, (1991) 160.

[7] E. Belau, et al., "Charge Collection in Silicon Strip Detectors", Nucl. Instr. and Meth. A214, (1983) 253.

[8] A. Peisert, "Silicon Microstrip Detectors" in Instrumentation in Elementary Particle Physics" ed. F. Sauli, World Scientific (1992).

[9] J. Carr et al., "Simulation of VDET", ALEPH 92-52, SOFTWR 92-06.

[10] G. Lutz, "Correlated Noise in Silicon Strip Detector Readout", Nucl. Instr. and Meth. A309, (1991) 545.

[11] S.Hancock, F.James, J.Movchet, P.G. Rancoita, L.VanRossum, *Physical Review* **A 28** (1983) 615

[12] A. Bonissent et al., "B-tagging improvements with the upgraded vertex detector", ALEPH 94-51, MINIV 94-02

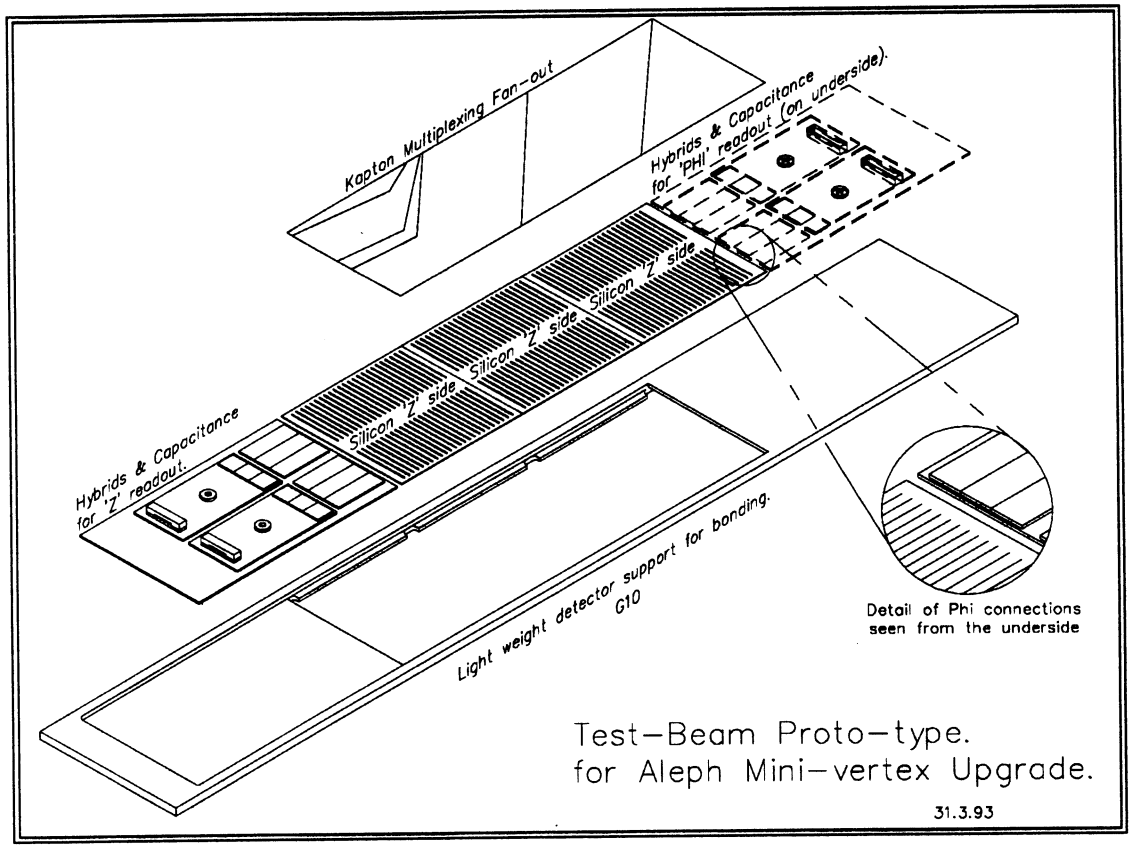

Figure 1: Schematic Drawing of a prototype module.

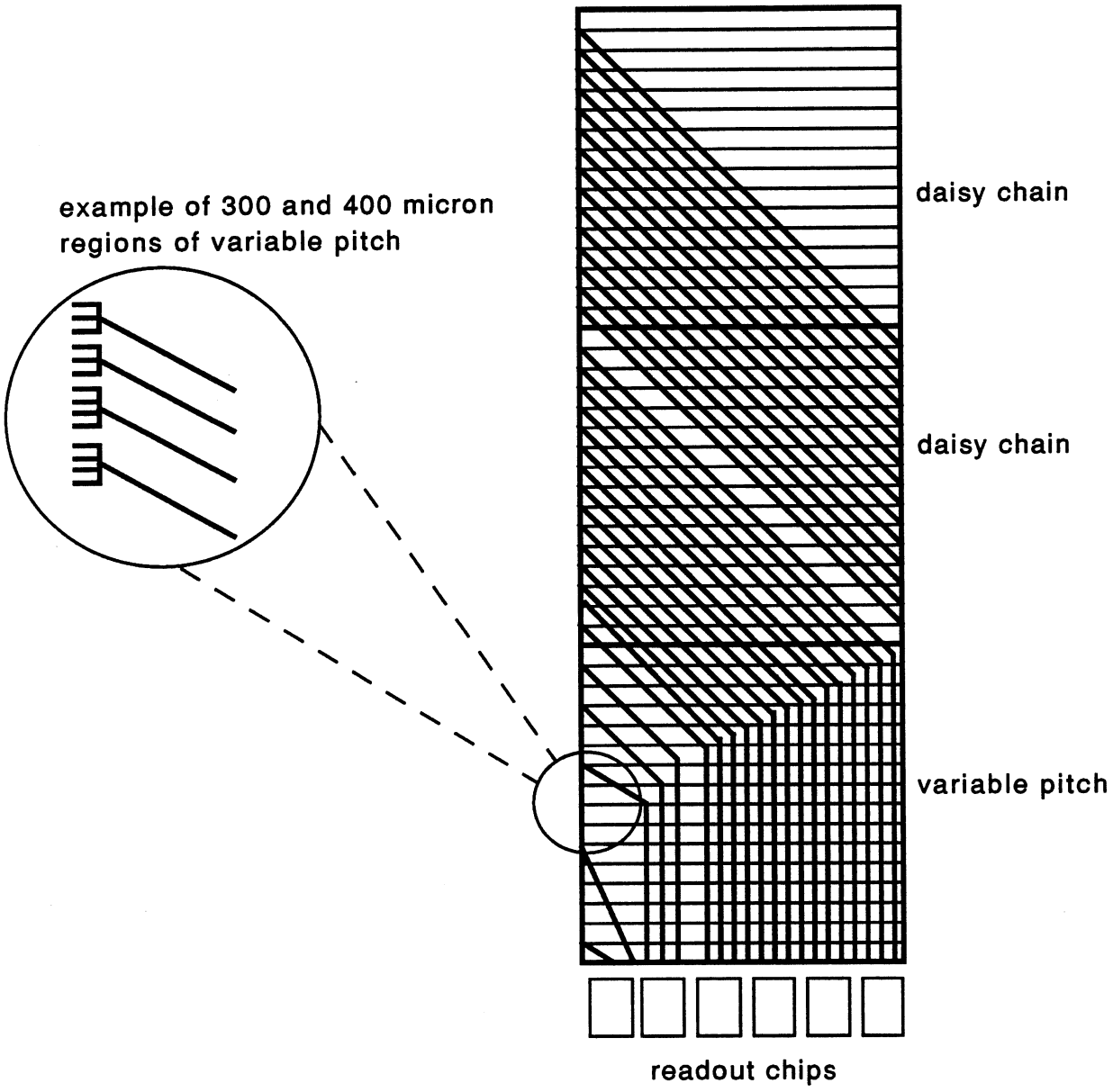

Figure 2: Schematic of the kapton z side fanout

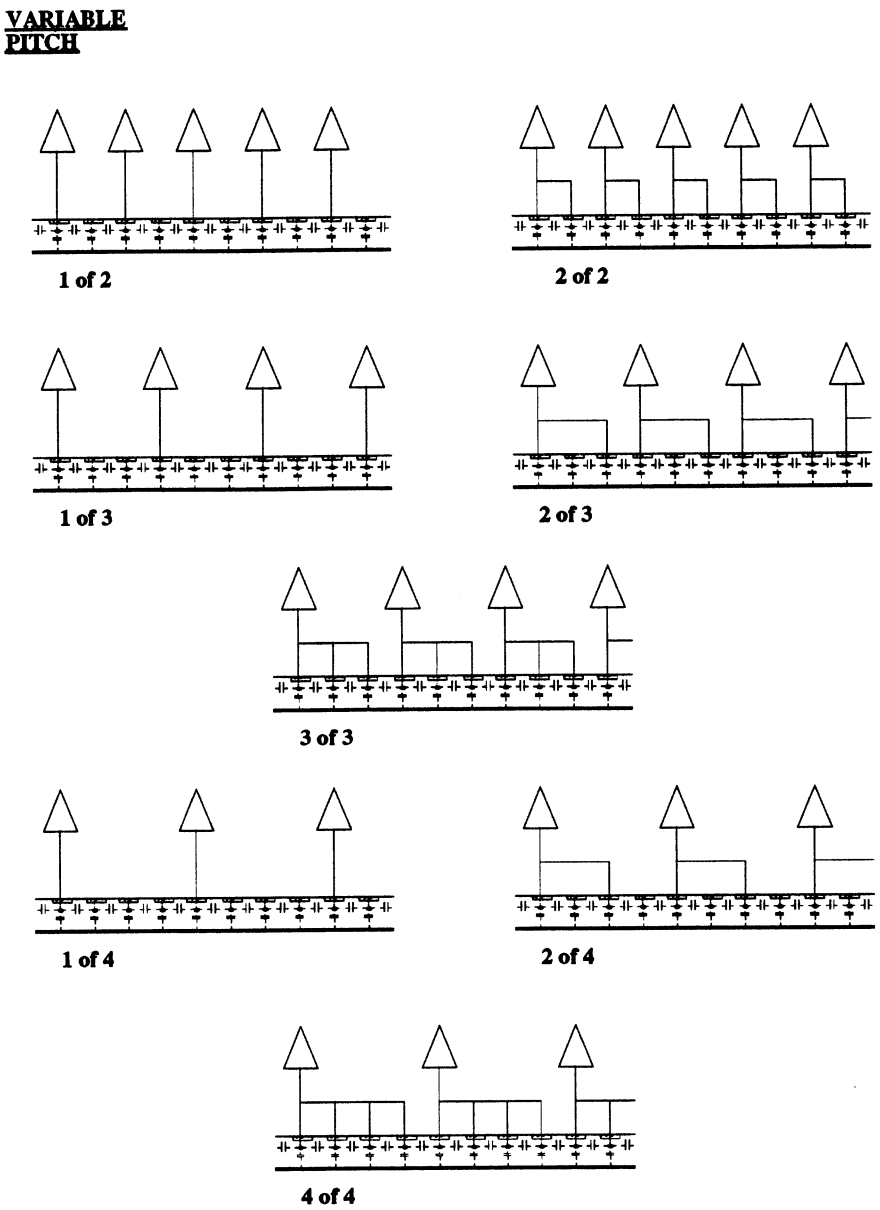

Figure 3: Connection schemes used in the variable pitch region. The interstrip and strip-to-ground capacitances are also indicated. For simplicity, only strips at $100\mu m$ pitch are shown. In between each pair an addition floating strip is present.

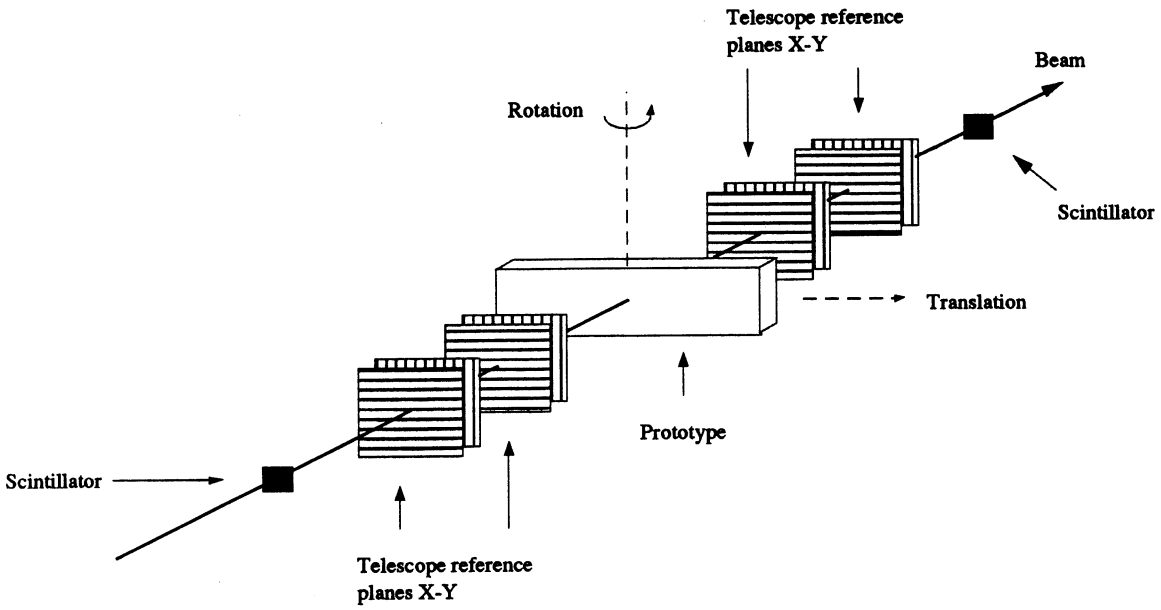

Figure 4: Schematic of the testbeam setup.

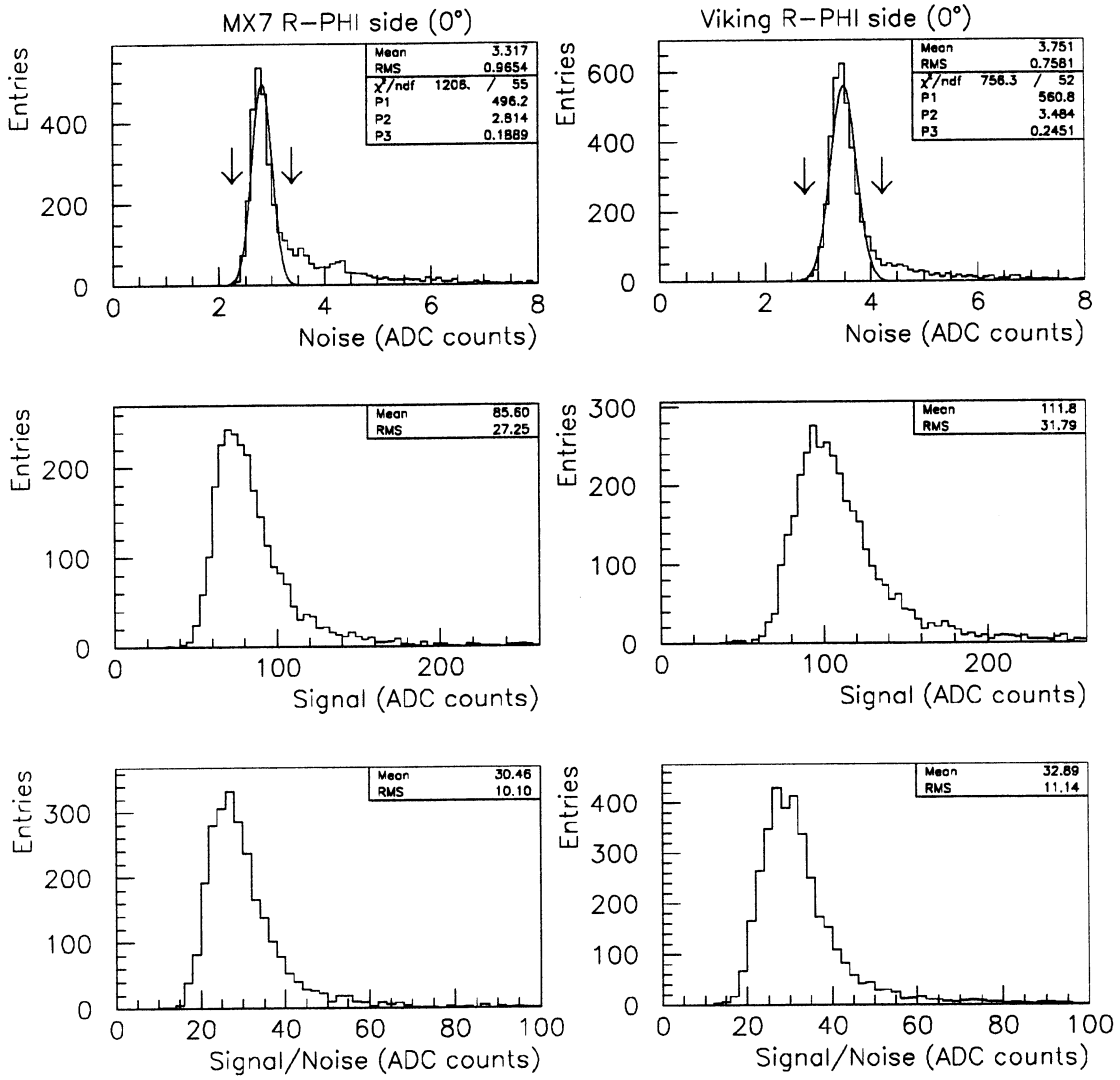

Figure 5: Distributions of the noise, signal and signal/noise for the MX7 and VIKING $r\phi$ side at zero degrees.

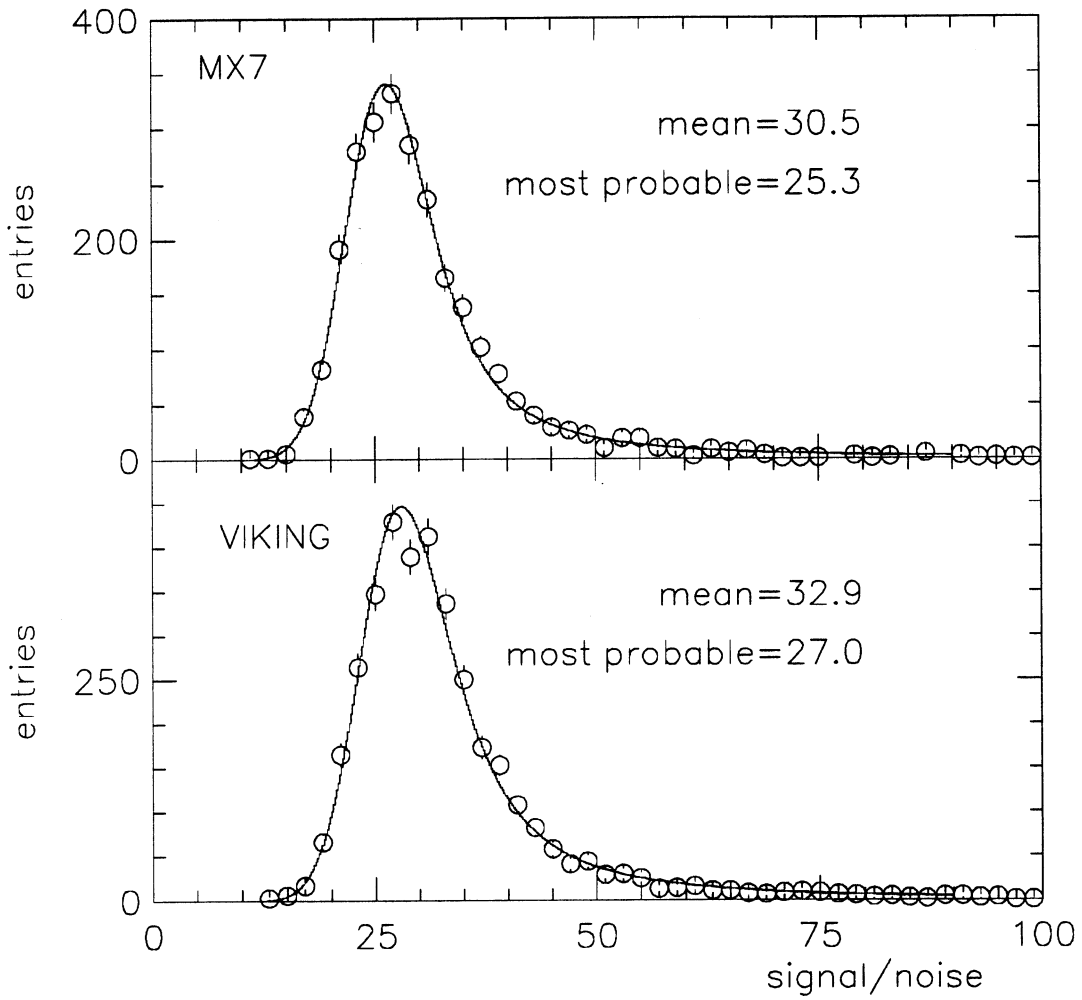

Figure 6: Landau fit to signal/noise of the MX7 and VIKING $r\phi$ side at zero degrees.

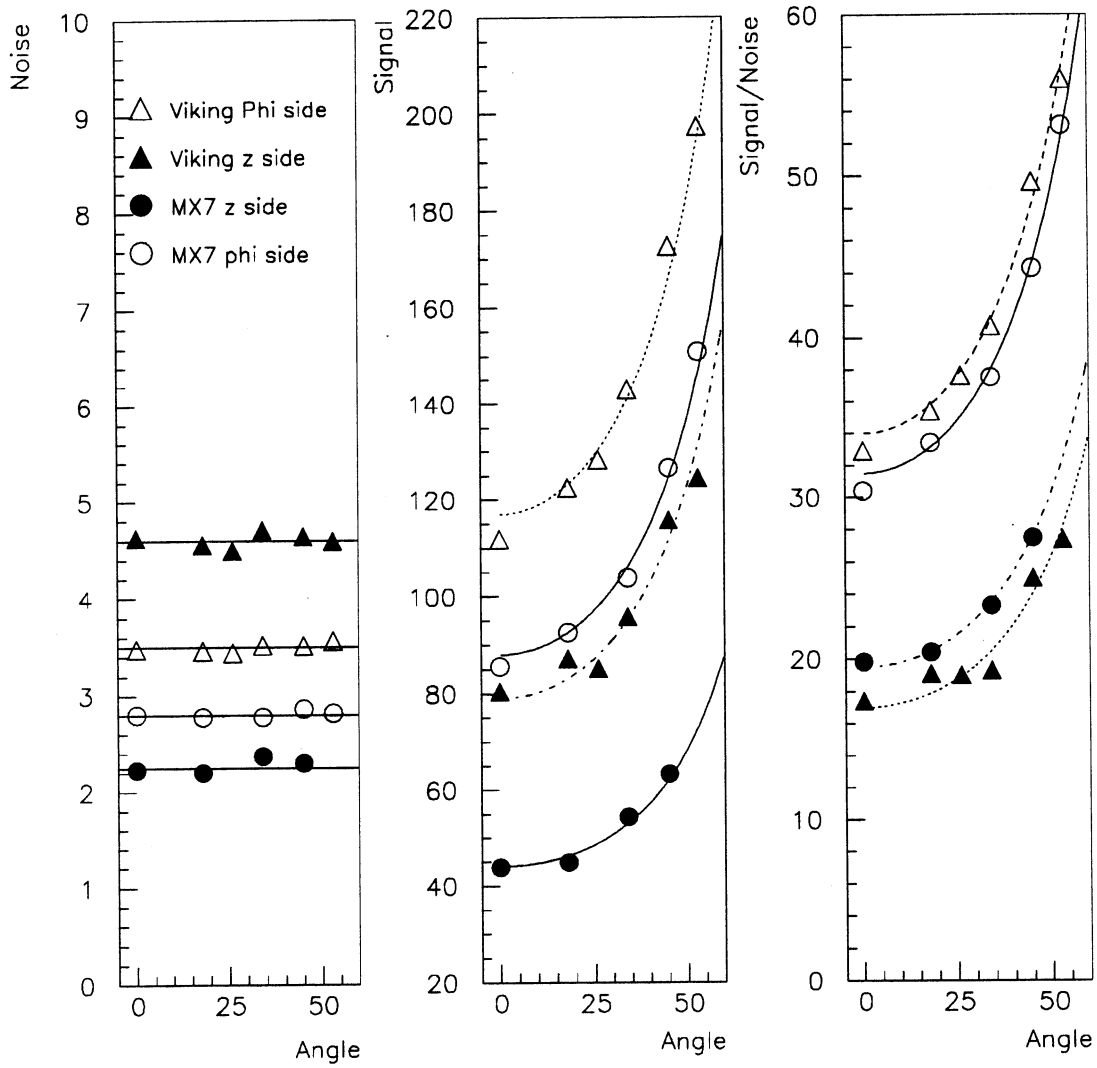

Figure 7: Signal, Noise, signal/noise for the $r\phi$ side and the z side (daisy chain) as a function of incident track angle.

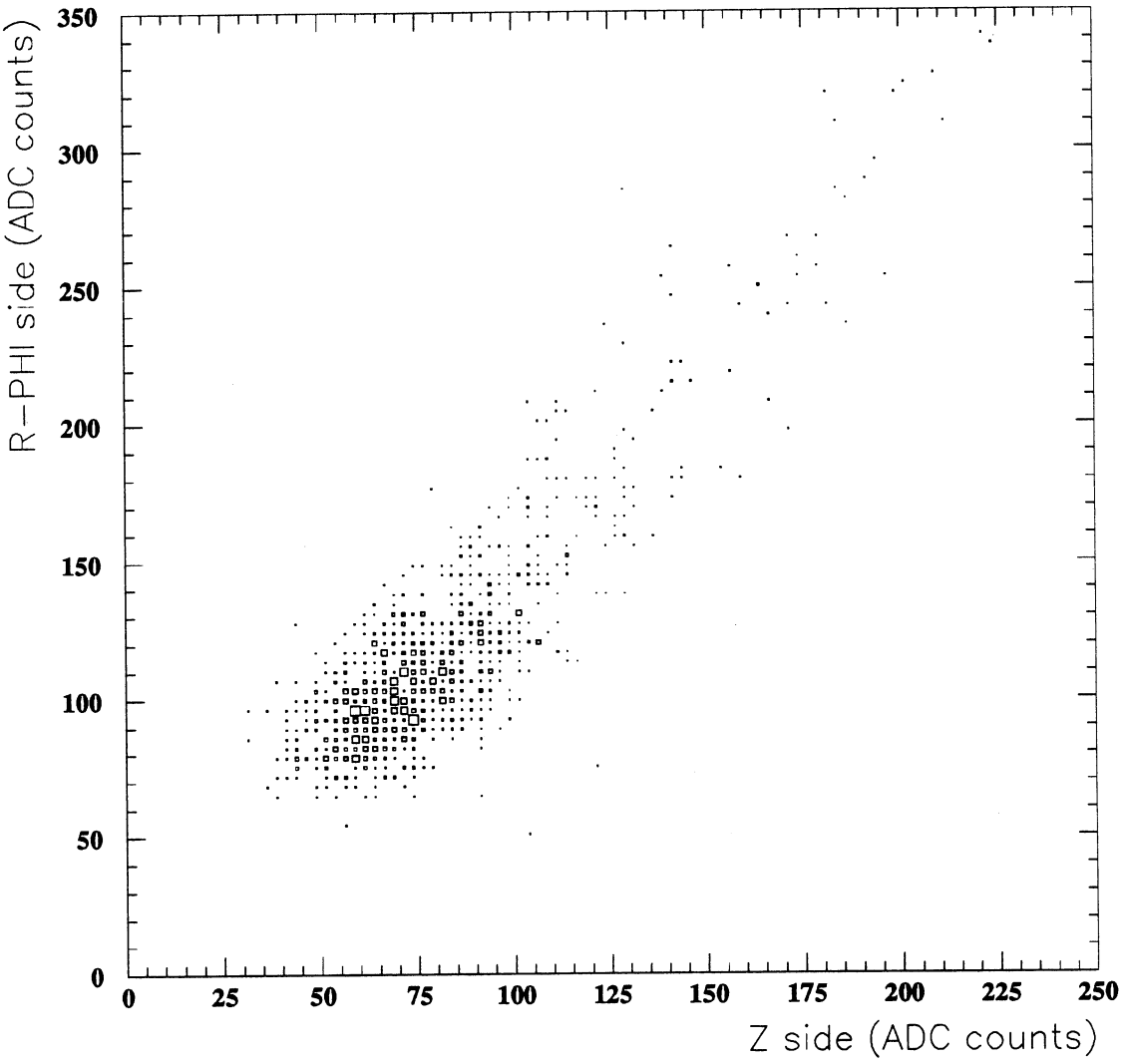

Figure 8: Pulse height correlation between the $r\phi$ and z sides.

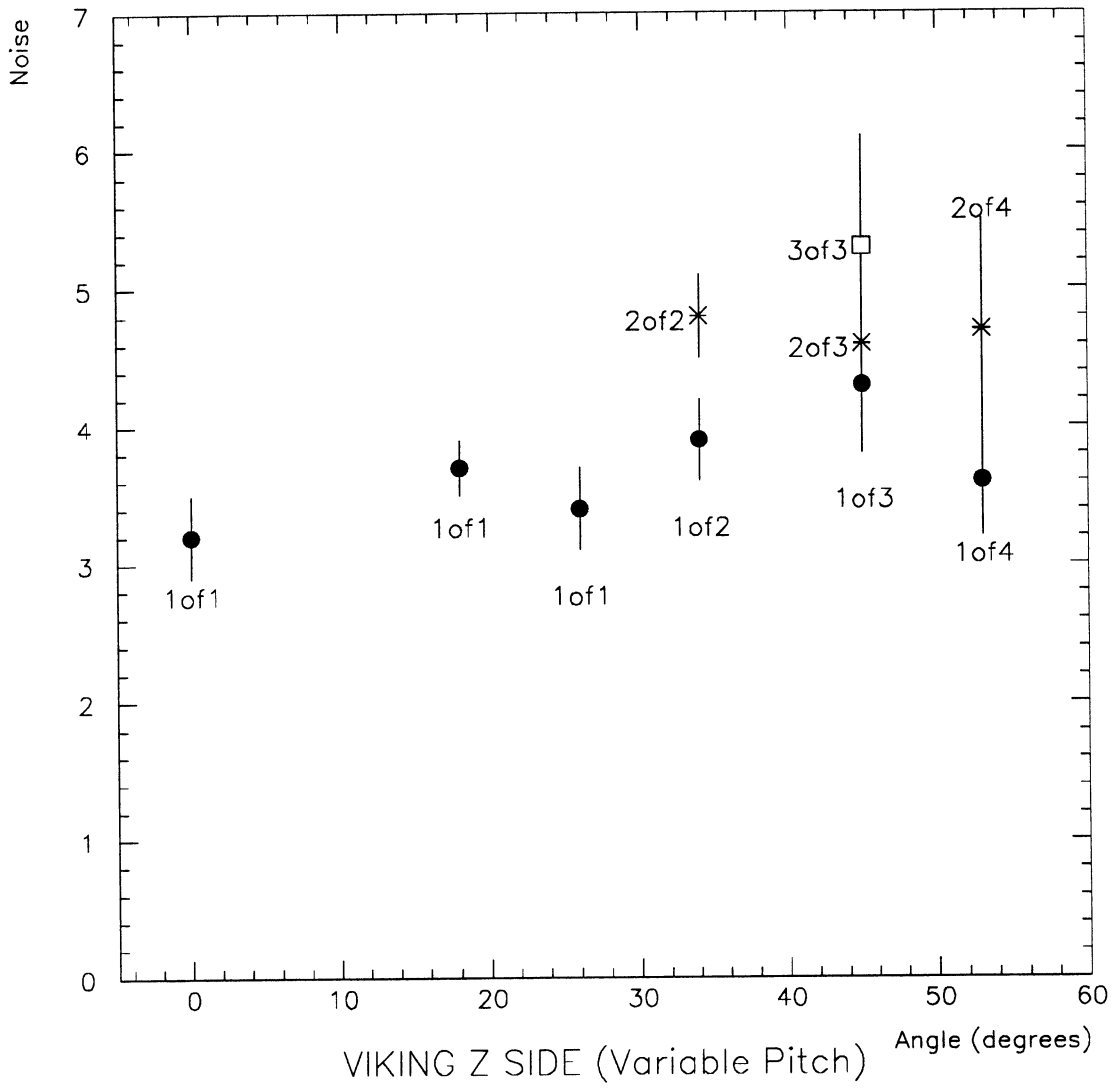

Figure 9: Noise versus angle and connection scheme for the VIKING z side variable pitch region.

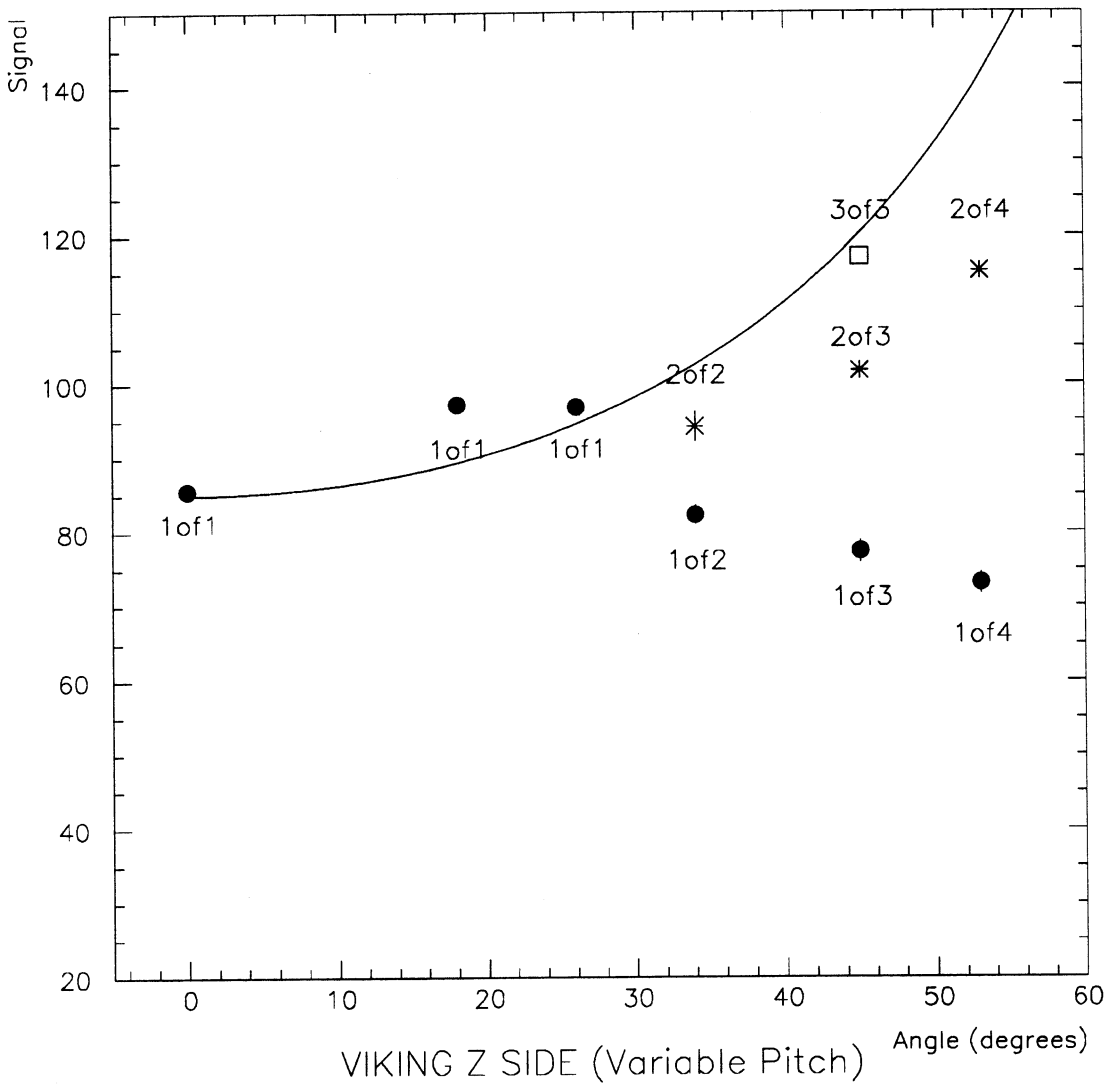

Figure 10: Signal versus angle and connection scheme for the VIKING z side variable pitch region.

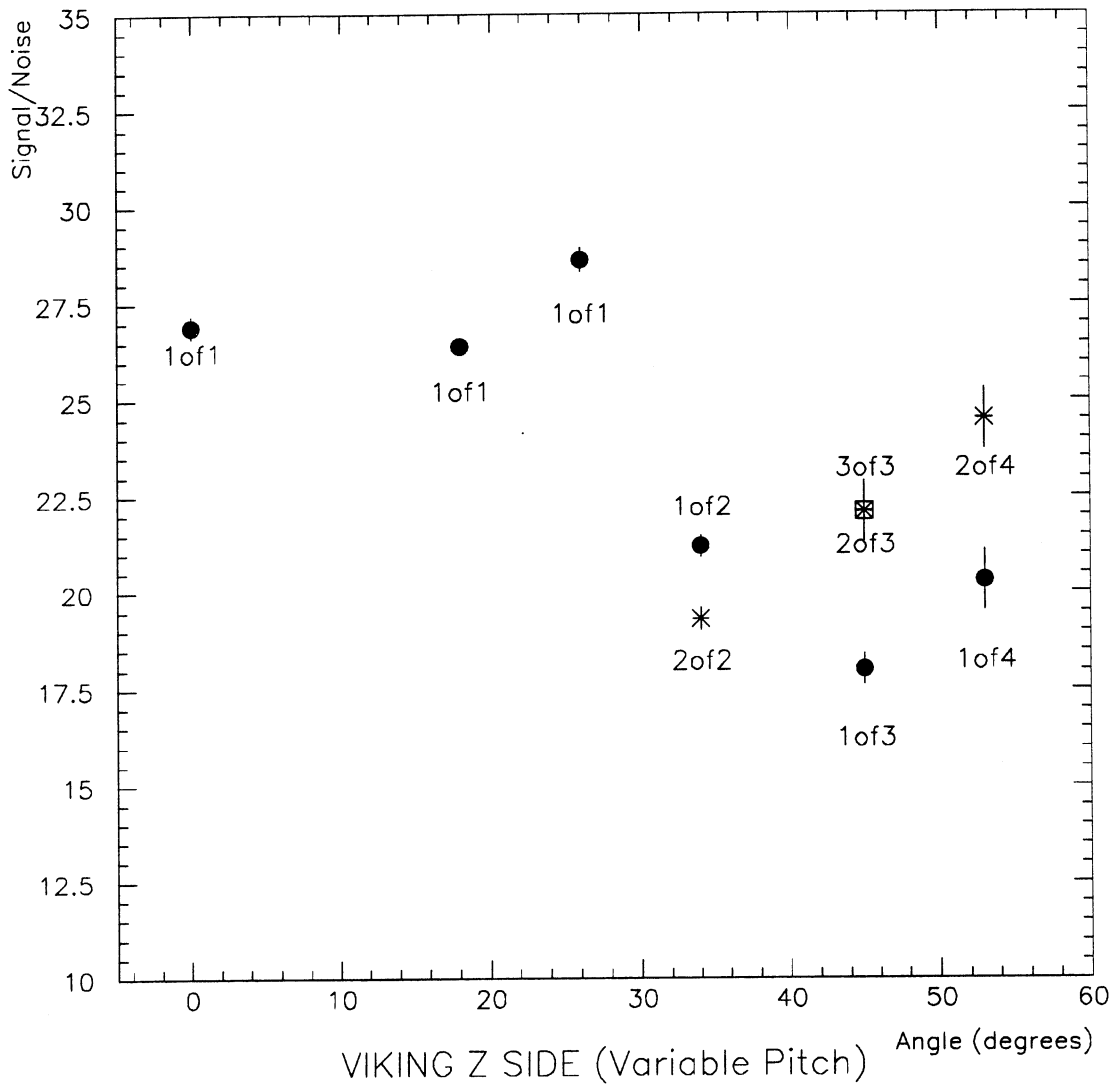

Figure 11: Signal/noise versus angle and connection scheme for the VIKING z side variable pitch.

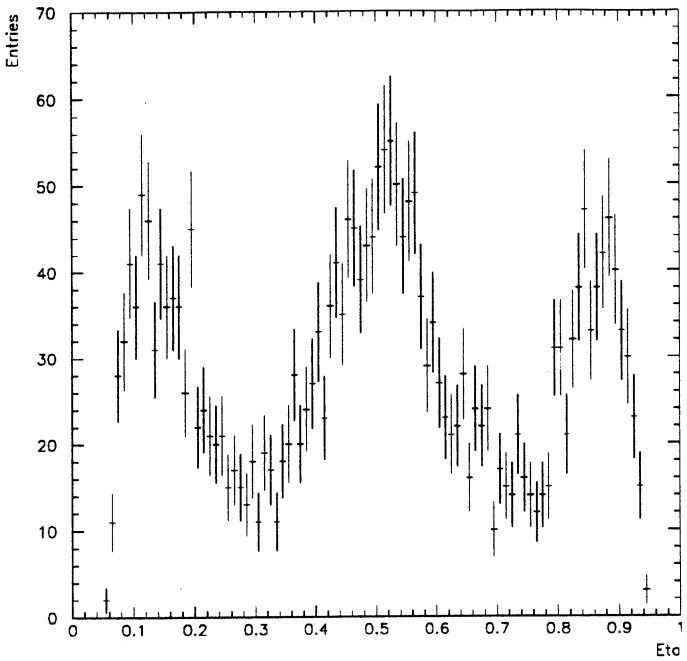

Figure 12: Histogram of η for perpendicularly incident tracks.

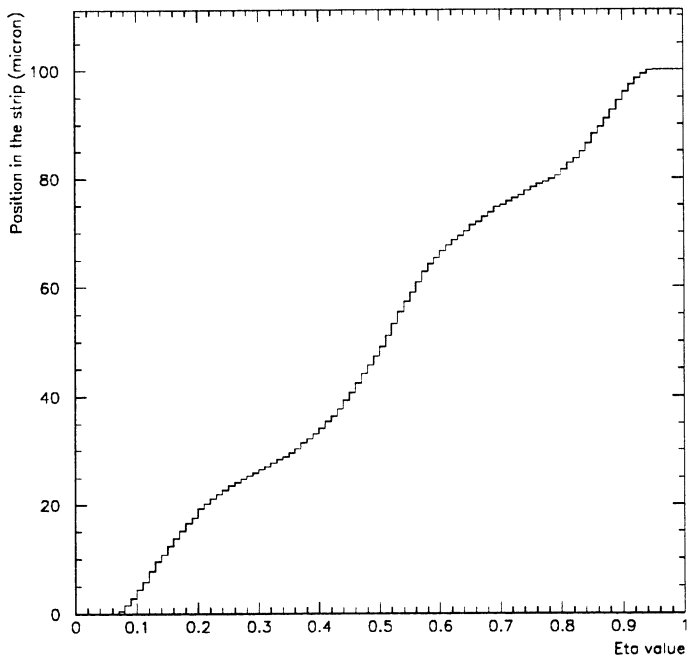

Figure 13: Normalised integrated η distribution.

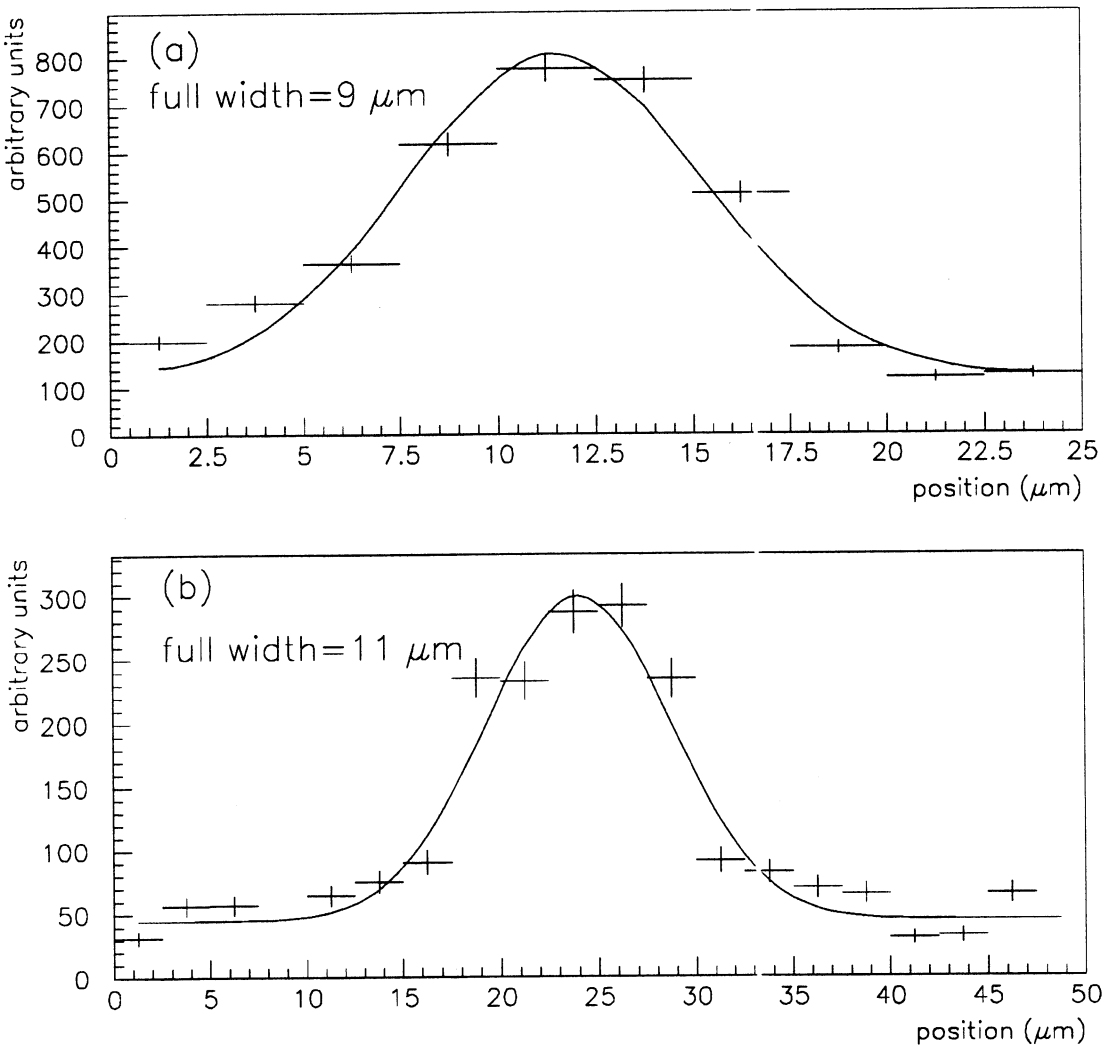

Figure 14: Calculated charge distribution for (a) the $r\phi$ side and (b) the z side.

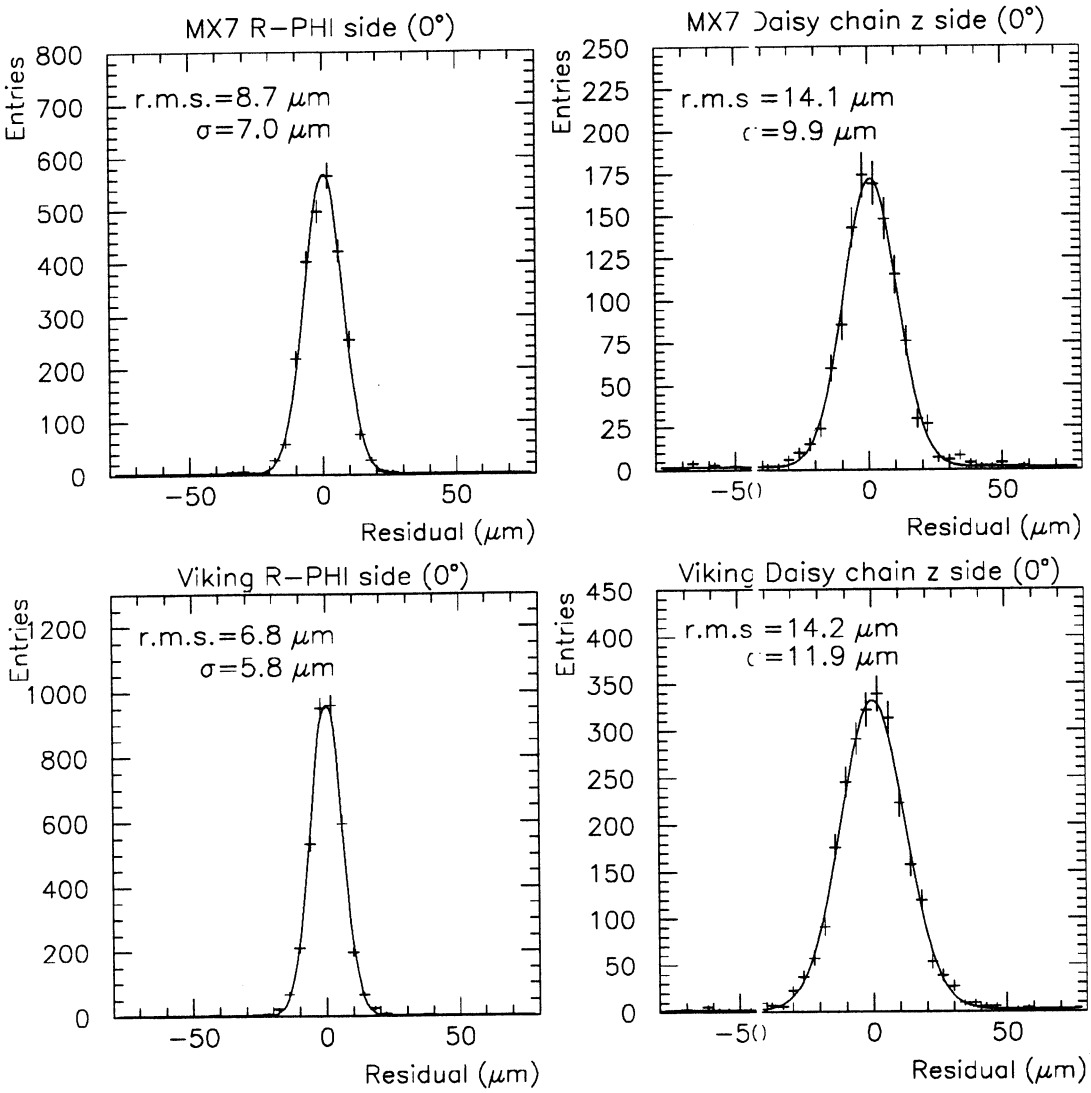

Figure 15: Gaussian fits to the distributions of the difference between the expected and measured track impact positions in the MX7 and VIKING prototypes for perpendicularly incident tracks.

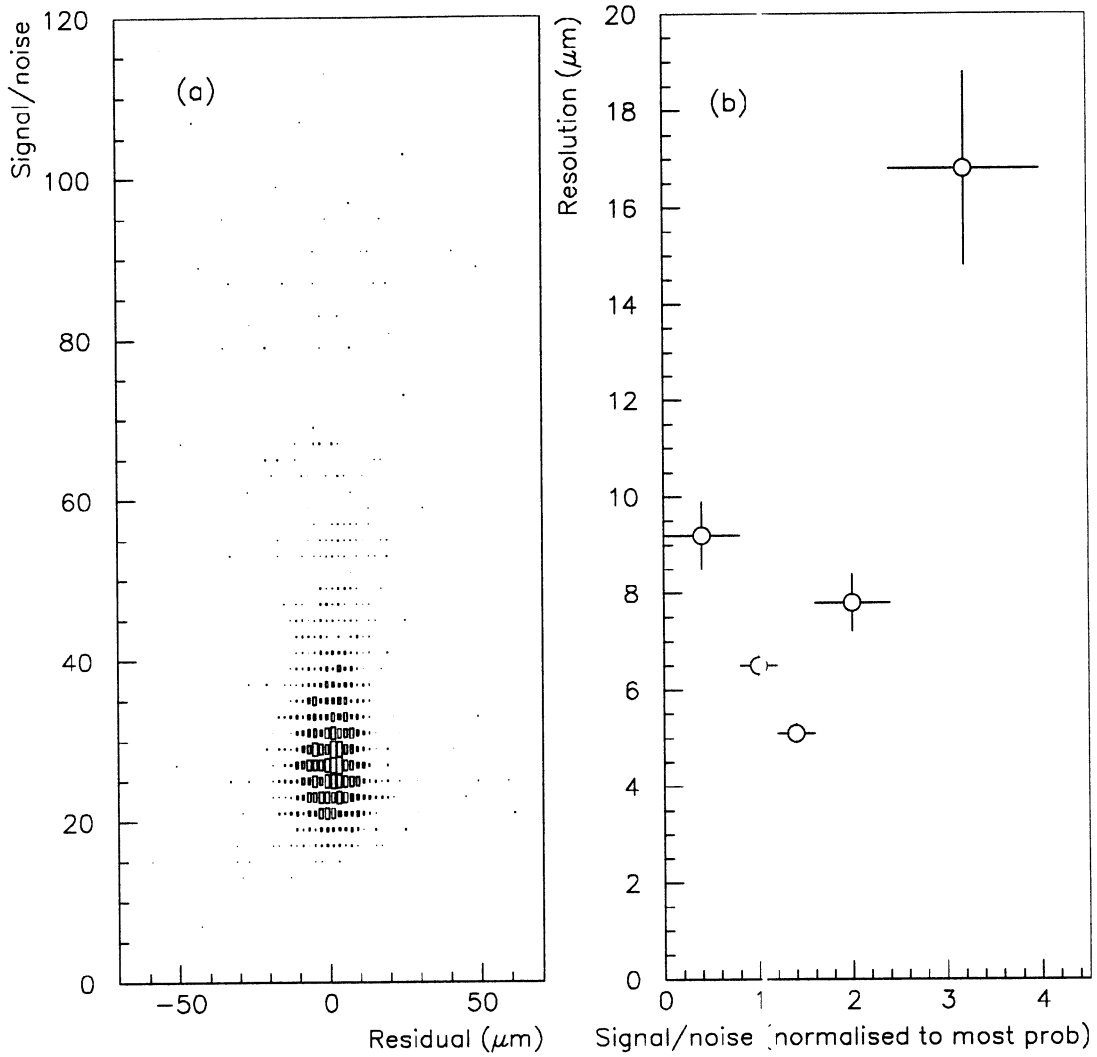

Figure 16: (a) Scatter plot of residual versus signal/noise. (b) The resolution obtained for various slices of signal/noise. VIKING prototype, $r\varphi$ side

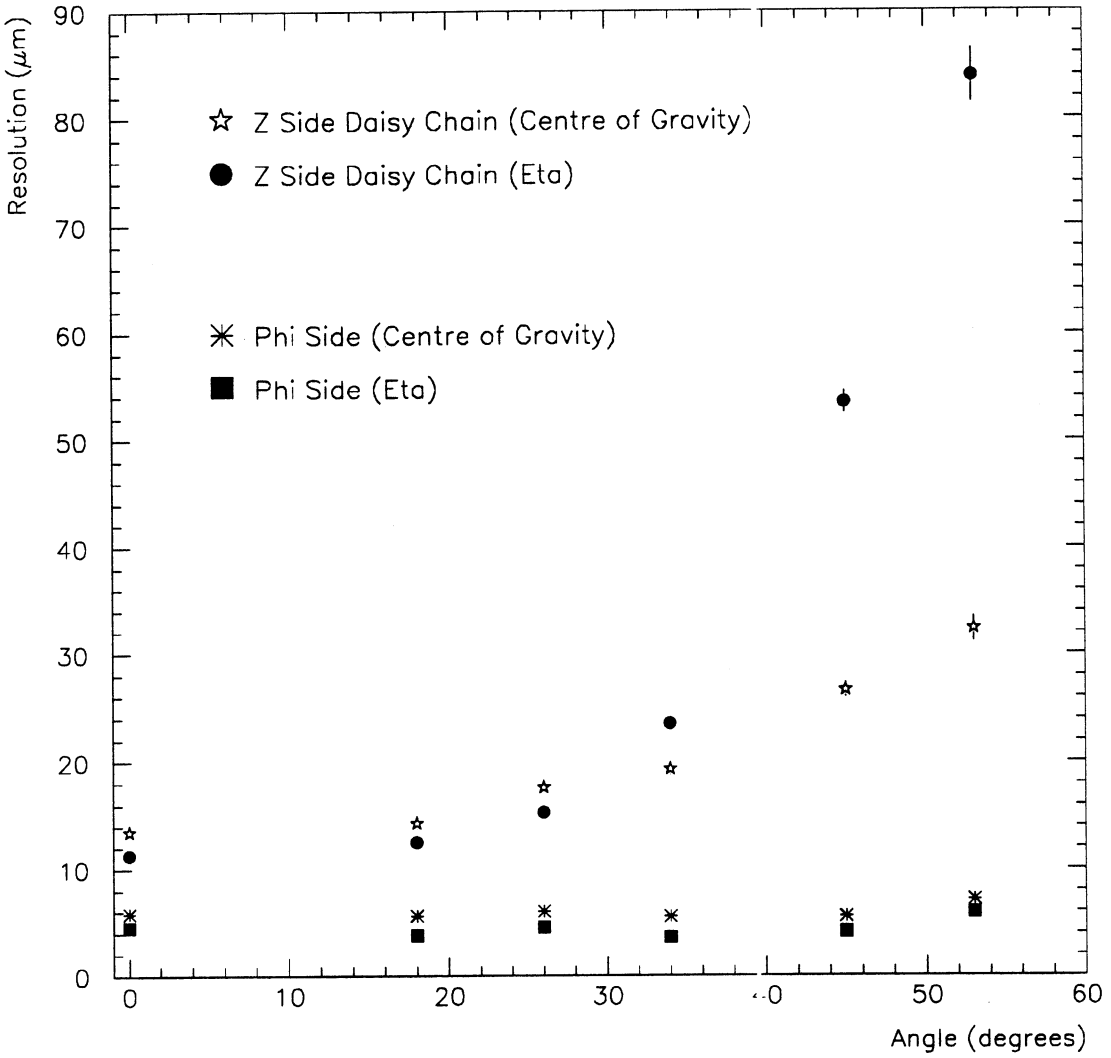

Figure 17: Position resolutions measured on the $r\phi$ and z sides (daisy chain) as a function of track angle, for the VIKING prototype. Results are shown using the centre of gravity and η algorithms.

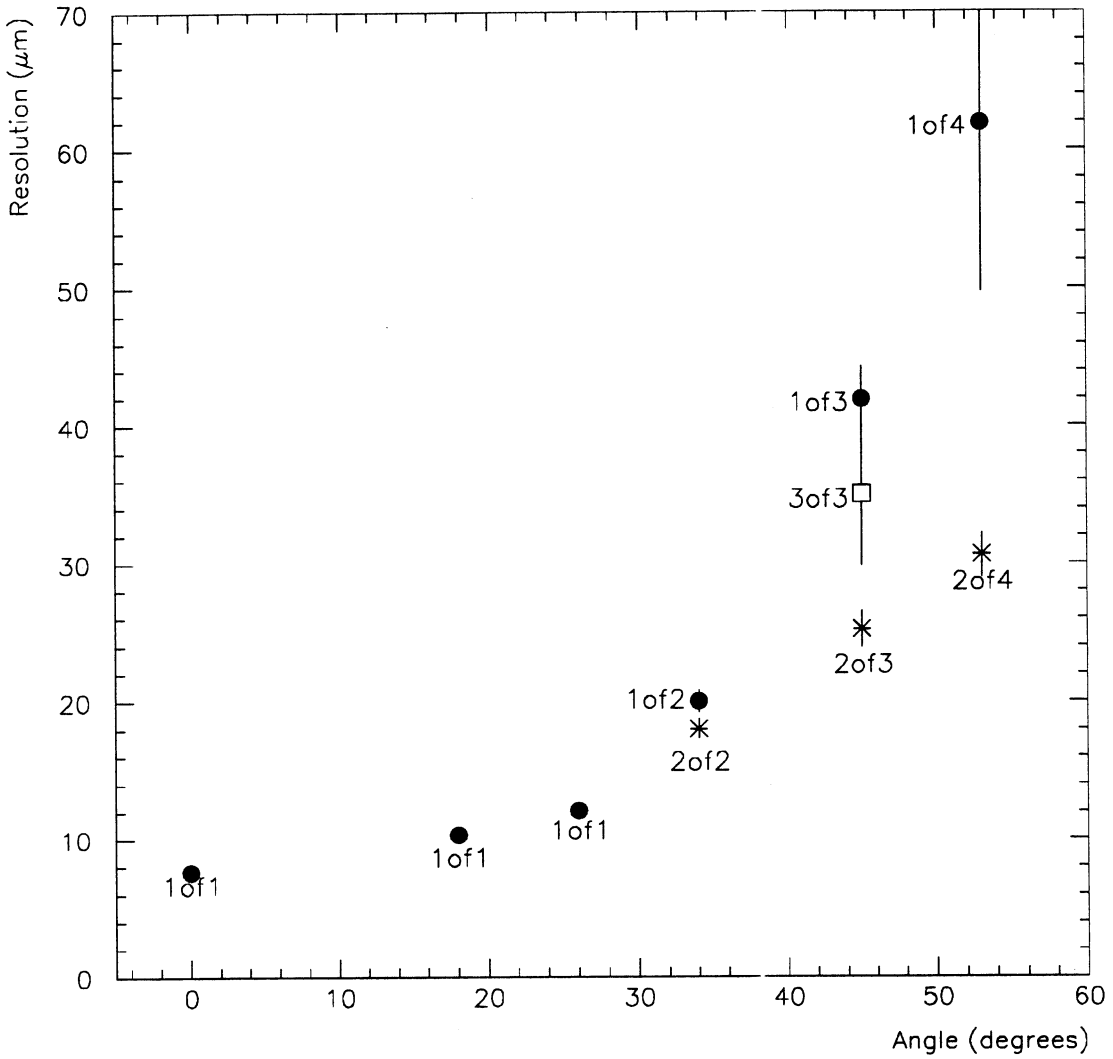

Figure 18: Resolutions measured on the z sides (variable pitch) as a function of track angle and connection scheme.

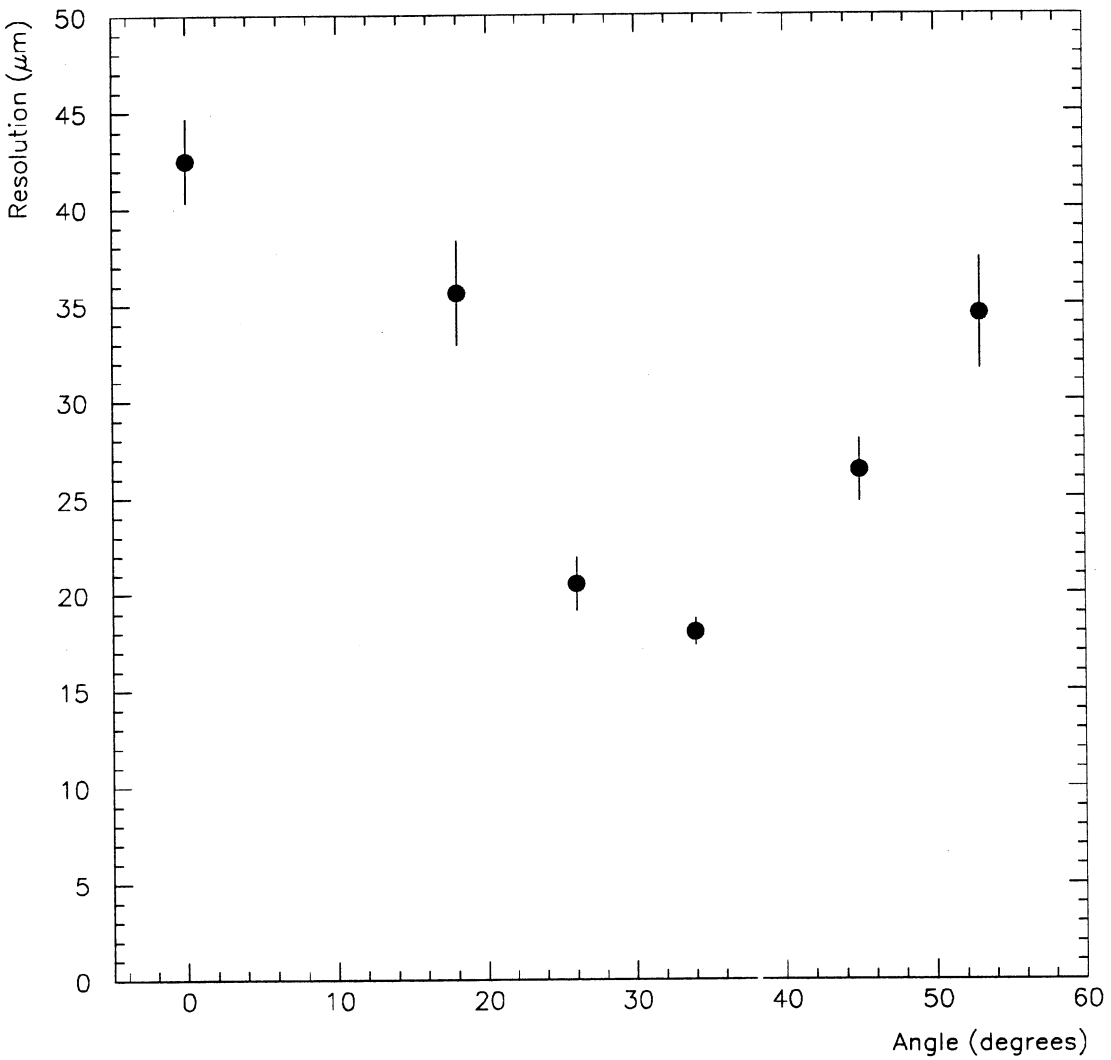

Figure 19: Effect on the resolution of having the wrong angle for the variable pitch region. (2-of-2 connection scheme.

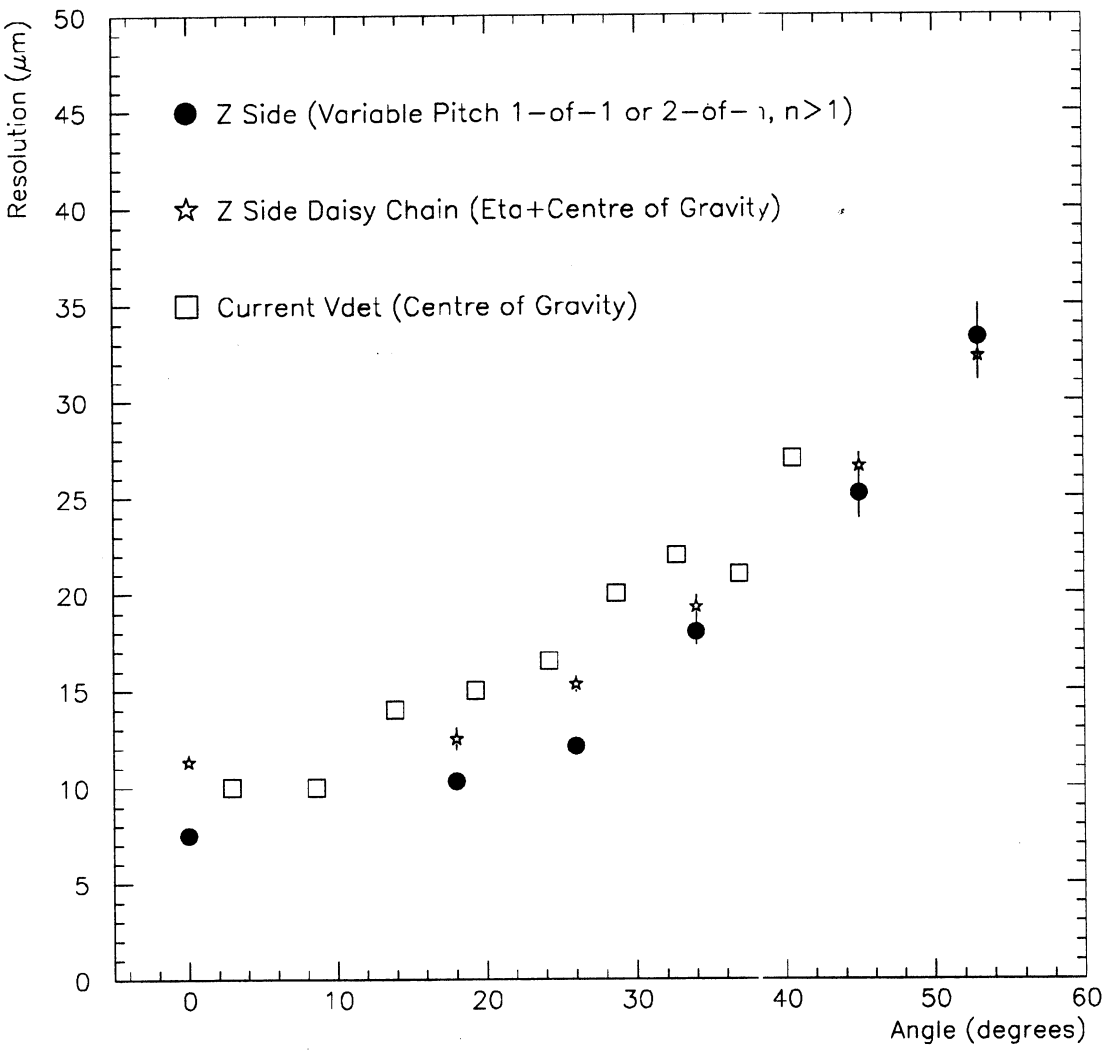

Figure 20: Comparision of the resolutions obtained on the z side using daisy chain and the best variable pitch (2-of-n) resolution. Also shown is the resolution measured in the data using the current Vdet.

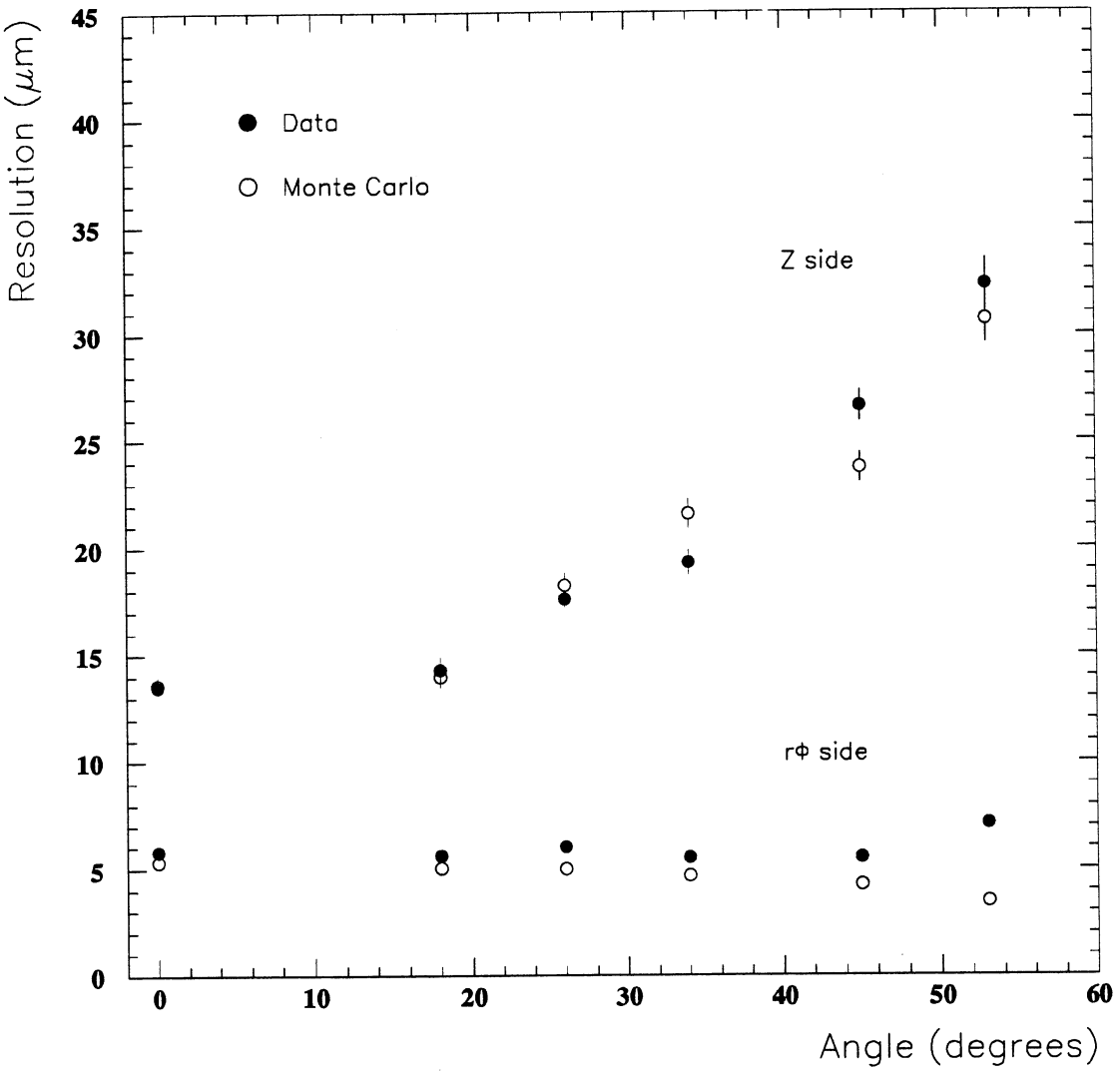

Figure 21: Comparision of position resolutions obtained from data and Monte Carlo (z and $r\phi$ sides) using the centre of gravity method. VIKING readout.

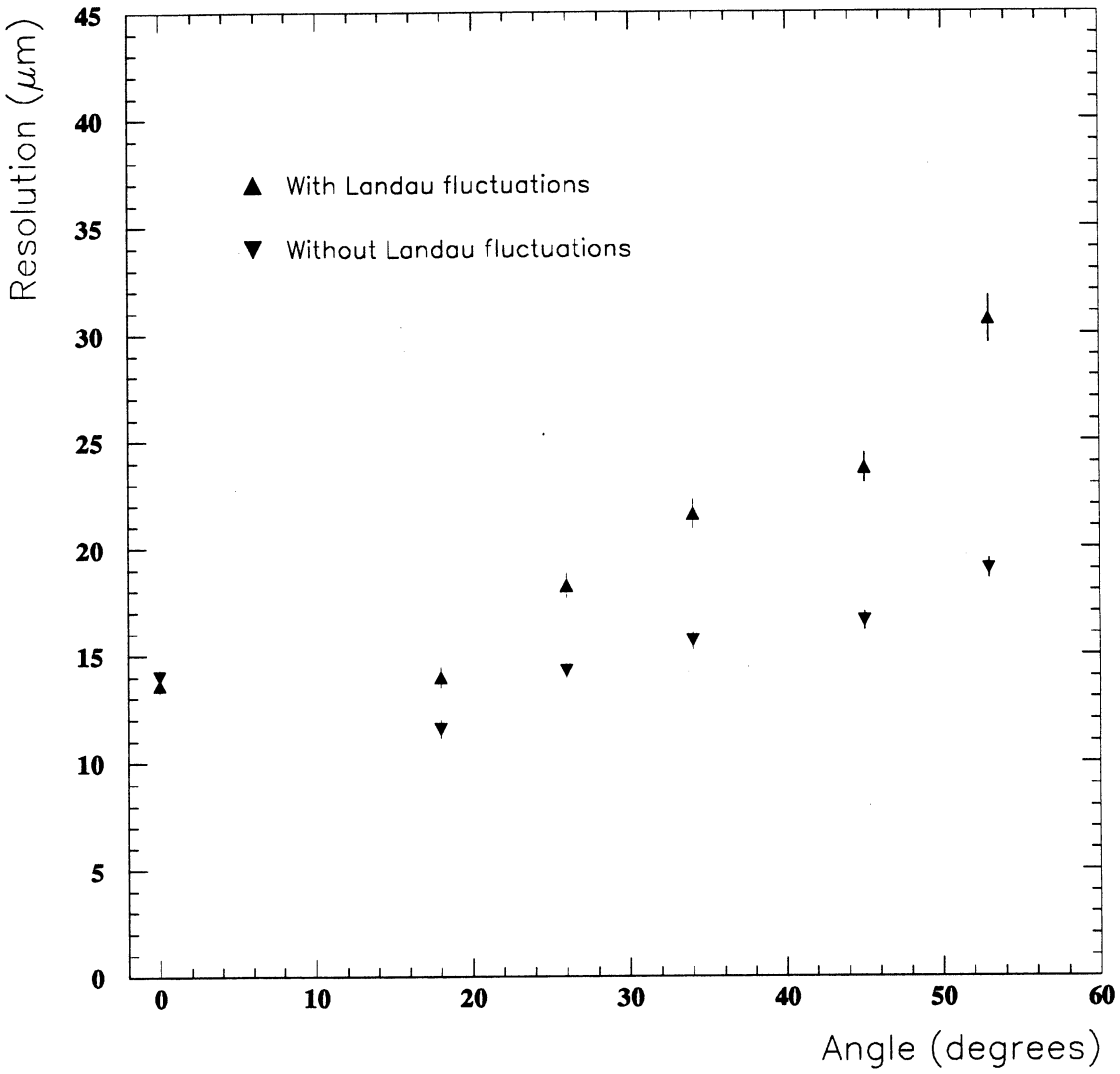

Figure 22: Effect of Landau fluctuations on the Monte Carlo resolution for the z side (daisy chain).